

Provenance and Paleo-weathering of the Mesozoic Rocks of Kutch Basin: Integrating Results from Heavy Minerals and Geochemical Proxies



Angana Chaudhuri, Emilia Le Pera, Gaurav Chauhan, and Santanu Banerjee

Abstract This study investigates the composition, tectonic setting and age of source rocks of the Mesozoic Kutch Basin, along with the extent of weathering based on heavy mineral characteristics and geochemical investigations. The Mesozoic succession, divided into Jhurio, Jhumara, Jhuran and Bhuj formations, preserves sediments deposited in the Kutch Basin from the Late Triassic to Early Cretaceous. Subangular and subrounded heavy minerals indicate mixing of first cycle and recycled input in these samples. Major oxide ratios such as $\text{SiO}_2/\text{Al}_2\text{O}_3$, $\text{Al}_2\text{O}_3/\text{TiO}_2$, $\text{K}_2\text{O}/\text{Na}_2\text{O}$ and trace elements like Zr, Th, Sc, Th/Co, Th/Sc and La/Sc indicate dominantly felsic source. LREE enrichments and negative Eu anomalies support the predominance of felsic source rocks. The V and Ni concentrations in these sediments indicate the input from mafic sources in the older Jhurio and Jhumara formations. Weathering indices such as CIA, PIA and CIW suggest the relatively greater extent of chemical alteration for Jhumara, Jhuran and Bhuj formations in comparison to Jhurio Formation. The higher content of Hf in Jhuran and Bhuj formations suggests the input from older source rocks in younger formations, indicating erosional unroofing at the source. The concentration of Cr and Ni and ratios of Eu/Eu* and $(\text{Gd}_N/\text{Yb}_N)$ indicate predominantly post-Archean source with inputs from older Archean rocks in younger Jhuran and Bhuj formations, and corroborate the erosional unroofing. These evidences relate possible sources of Mesozoic sediments in the Kutch Basin to Precambrian rocks of the Aravalli craton and Nagar Parkar igneous complex.

A. Chaudhuri (✉) · S. Banerjee

Department of Earth Sciences, Indian Institute of Technology Bombay, Powai, Mumbai 400076, India

S. Banerjee

e-mail: santanu@iitb.ac.in

E. Le Pera

Dipartimento di Biologia, Ecologia e Scienze della Terra, Università della Calabria, 87036 Rende, Cosenza, Italy

e-mail: emilia.lepera@unical.it

G. Chauhan

Department of Earth and Environmental Science, KSKV Kachchh University, Bhuj 370001, Gujarat, India

Keywords Provenance · Mesozoic · Kutch Basin · Paleo-weathering · Geochemistry

1 Introduction

Sedimentary rocks preserve information of their source rock, tectonic setting, paleodrainage and paleoclimatic conditions. Detailed thin section petrography of rock samples is a preliminary and routine step, especially for understanding provenance of siliciclastic sedimentary rocks (Crook 1974; Dickinson and Suczek 1979; Dickinson 1985; Zuffa 1987; Critelli and Ingersoll 1994; Le Pera et al. 2001; Critelli et al. 2003; Chaudhuri et al. 2018, 2020a). Further, the sedimentary rocks bear geochemical signatures of the source rocks (Quinby-Hunt and Wilde 1991; Ochoa et al. 2007). Major, trace, rare earth element concentrations and their ratios serve as proxies for composition, tectonic setting and age of source as well as the climate prevailing during deposition (Paikaray et al. 2008; Saha et al. 2010, 2018; Mondal et al. 2012; Armstrong-Altrin et al. 2017; Chaudhuri et al. 2020a, b). The concentration of major oxides and their ratios such as $\text{SiO}_2/\text{Al}_2\text{O}_3$, $\text{Al}_2\text{O}_3/\text{TiO}_2$, $\text{K}_2\text{O}/\text{Na}_2\text{O}$ are useful indicators of source rock characteristics (McLennan et al. 1979; Maynard et al. 1982; Roser and Korsch 1986; Hayashi et al. 1997). Trace element ratios, such as, La/Th, La/Sc, Th/Sc, Th/Co, Ti/Zr, Sc/Cr, La/Y are also useful for provenance interpretations (Bhatia and Crook 1986; Floyd and Leveridge 1987; McLennan et al. 1993; Cullers 2002). Indices such as CIA, PIA, CIW and ICV suggest the extent of weathering of source rock and prevailing climate at source area (Nesbitt and Young 1982; Harnois 1988; Fedo et al. 1995; Cox et al. 1995).

The Kutch Basin at the western continental margin of India preserves ~3000 m of Mesozoic sediments deposited during the breakup of Gondwana and the subsequent drift of the Indian subcontinent (Biswas 1982, 1987, 2005). Several studies provided insights on provenance for the Mesozoic succession of the Kutch Basin, although based on a limited dataset (Ahmad and Bhat 2006; Ahmad et al. 2014; Periasamy and Venkateshwarlu 2017). Recently Chaudhuri et al. (2018, 2020a, b, c, d) presented sandstone petrography, single-grain heavy mineral analysis, geochemistry of trace elements, Nd isotopes in shale and geochronology of detrital zircon and monazite. However, data collected from different rock types using different methods need to be integrated. The present study aims to understand the composition, tectonic setting and age of source rocks of the Mesozoic sediments in the Kutch Basin and assess the extent of weathering at the source. This paper integrates petrographical, geochemical and geochronological data to accomplish this objective. Already published petrographic data have been considered for interpretation.

2 Geological Setting

The Mesozoic Kutch Basin formed due to the rifting of the Gondwana supercontinent (Biswas 1982, 1987, 2005). Nagar Parkar Ridge to the north, Kathiawar Uplift to the south, Radhanpur-Barmer Arch to the east and the continental shelf to the west demarcates the Kutch Basin. The vast thickness of Mesozoic sedimentary rocks of this basin crops out in several uplifts, viz., Nagar Parkar Uplift (NPU), Island Belt Uplift (IBU), South Wagad Uplift (SWU) and Kutch Mainland Uplift (KMU). The KMU is the largest uplift preserving Late Triassic to Early Cretaceous mixed siliciclastic sediments (Alberti et al. 2013).

The Mesozoic succession in the KMU comprises Jhurio, Jhumara, Jhuran and Bhuj formations in ascending order of succession (Biswas 1987) (Fig. 1). The Bathonian to early Callovian carbonates and finer siliciclastics, classified as the Jhurio Formation overlies unconformably on the Precambrian basement rocks. The younger Oxfordian sediments of the Jhumara Formation comprise argillaceous rocks at the bottom and carbonates at the top (Biswas 2005). The Kimmeridgian to Tithonian sediments of the Jhuran Formation overlies unconformably on the Jhumara Formation. The alternation between sandstone and shale makes up the overall prograding Jhuran Formation (Arora et al. 2015). The Neocomian to Albian siliciclastics of the Bhuj Formation unconformably overlie the Jhuran Formation. Although the older carbonate and finer clast-dominated formations do not show much paleocurrent

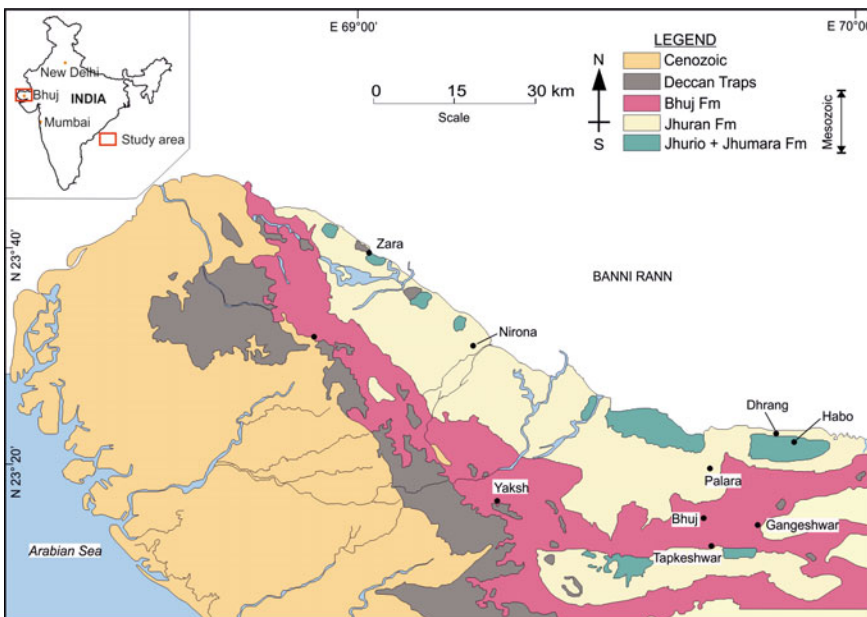


Fig. 1 Geological map of Kutch Mainland showing extent of Mesozoic and Cenozoic sedimentary rocks (adapted from Biswas 1977, 1981)

structures, the younger, siliciclastics-dominated Jhuran and Bhuj formations provide a south-westerly paleoslope (Biswas 1991, 1993, 2005; Arora et al. 2015; Mandal et al. 2016; Bansal et al. 2017; Desai and Biswas 2018).

3 Methods

Sandstone and shale samples of Jhurio, Jhumara, Jhuran and Bhuj formations were collected from outcrops at Zara, Nirona, Yaksh, Dhrang, Habo, Palara, Gangeshwar, Tapkeshwar and Bhuj. These samples were crushed and dry sieved to separate the 63–125 μm size fraction. 10 gm of each of the sieved samples was poured into a beaker. The beaker was filled with water and the sample was allowed to settle. The lighter clay minerals and water from the upper part of the beaker were decanted into a large bowl. The beaker was again filled with water and the contents were agitated by swirling. The upper part of the beaker was once again emptied in the large bowl. This process was repeated several times to concentrate the heavy minerals. The contents were then transferred to a watch glass, swirled slowly to concentrate the heavy minerals in the deepest part of the beaker. The light minerals and the extra water was siphoned off using a dropper. The dried heavy minerals were observed using Leica DM 4500P polarizing microscope attached with Leica DFC420 camera and Leica Image Analysis software (LAS-v4.6) at the Department of Earth Sciences, Indian Institute of Technology Bombay. Heavy minerals were identified using optical properties described by Mange and Maurer (2012). Sandstone samples were excluded for geochemical analysis because of both extensive cementation, that commonly results in removal of unstable framework components (e.g. Worden and Burley 2003), and the growth of authigenic phases changing the original detrital phases (e.g. Scholle and Schluger 1979; McDonald and Surdam 1984).

Shale samples were exclusively chosen for the geochemical analyses. For major oxide analyses, 0.25 g of each sample powder ($<63 \mu\text{m}$) was added to 0.75 g lithium metaborate (LiBO_2) and 0.50 g of lithium tetraborate (LiB_4O_7) in a platinum crucible. This mixture was fused in a muffle furnace at 1050 °C for 10 min. The temperature of the furnace was then lowered to 800 °C. The crucible was removed from the furnace, immersed in 75 ml of 1N HCl in a glass beaker and magnetically stirred for 1 h until complete dissolution of the fusion bead. This solution was transferred into a 100 ml volumetric flask. 1N HCl was added to the flask to make the volume 100 ml. 5 ml of this solution was diluted to 50 ml with distilled water for analysis using Inductively Coupled Plasma Atomic Emission Spectrometry (ICP-AES) (ARCOS, Simultaneous ICP Spectrometer by SPECTRO® Analytical Instruments GmbH, Germany) facility at the Sophisticated Analytical Instrument Facility (SAIF), Indian Institute of Technology Bombay. USGS standards, MAG-1, SBC-1, SCo-1 and SCo-2 were used for the analysis. Loss on ignition (LOI) was measured and calculated using the weight loss of 1 g of sample on heating to 950 °C.

For determining trace element (TEs) concentrations, including those of rare-earth elements (REEs), 0.05 g of each sample powder ($<63 \mu\text{m}$) was poured into individual

Savillex Teflon pressure decomposition vessels (25 ml). Ten ml of an acid mixture with HF/HNO₃ = 7:3 was added to each vessel. The content of the vessel was mixed thoroughly by swirling and heated at ~160 °C for 48 h. A few drops of HClO₄ was added to the content and evaporated at 200 °C to near dryness. Ten ml of an acid mixture with HNO₃/Milli Q® de-ionized water = 1:1 was added to the vessel and mixed thoroughly. The vessel was tightly closed and heated at 80 °C for 30 min. The sample solution was poured into a 250 ml volumetric flask. Five ml of 1 ng/ml ¹⁰³Rh solution was added to this flask as an internal standard. Further, Milli Q® de-ionized water was added to make the volume of content in the flask to 250 ml. Five ml of sample solution from each of the 250 ml flasks was diluted to 50 ml using Milli Q® de-ionized water for analysis by high resolution inductively coupled mass spectrometer (HR-ICP-MS) (Attom ES by Nu Instruments®, UK) along with the instrument software (Attolab v.1), at CSIR-National Geophysical Research Institute (NGRI), Hyderabad. USGS standard reference materials, MAG-1, SBC-1, SCo-1 and SCo-2 were used for analysis. Chinese standard reference material, GSR-5 was used to check the accuracy of the analysis. The data processing was done using Nu Quant®.

4 Results

4.1 Heavy Minerals

Sandstones of the Jhurio, Jhumara, Jhuran and Bhuj formations contain heavy minerals with both subangular and subrounded grains (Fig. 2). The most common transparent heavy minerals in these sandstones, in order of decreasing abundance, are ultrastable phases such as zircon, tourmaline, rutile (e.g. Hubert 1962), stable phases such as garnet, monazite and apatite, and less common moderately stable species such as epidote. Zircon grains are dominantly colourless or pale pink, with a few brown varieties (Fig. 2a). Tourmaline grains exhibit greenish-brown to greyish-blue colours (Fig. 2b). Rutile occurs in reddish-brown to amber-brown colours (Fig. 2c). Epidote occurs in yellow, while apatite exhibits colourless to light-grey (Fig. 2d, e). Monazite grains exhibit pale yellowish-brown colours (Fig. 2f). This diverse heavy mineral assemblage does not exhibit any significant corrosion, implying insignificant dissolution during the burial diagenesis.

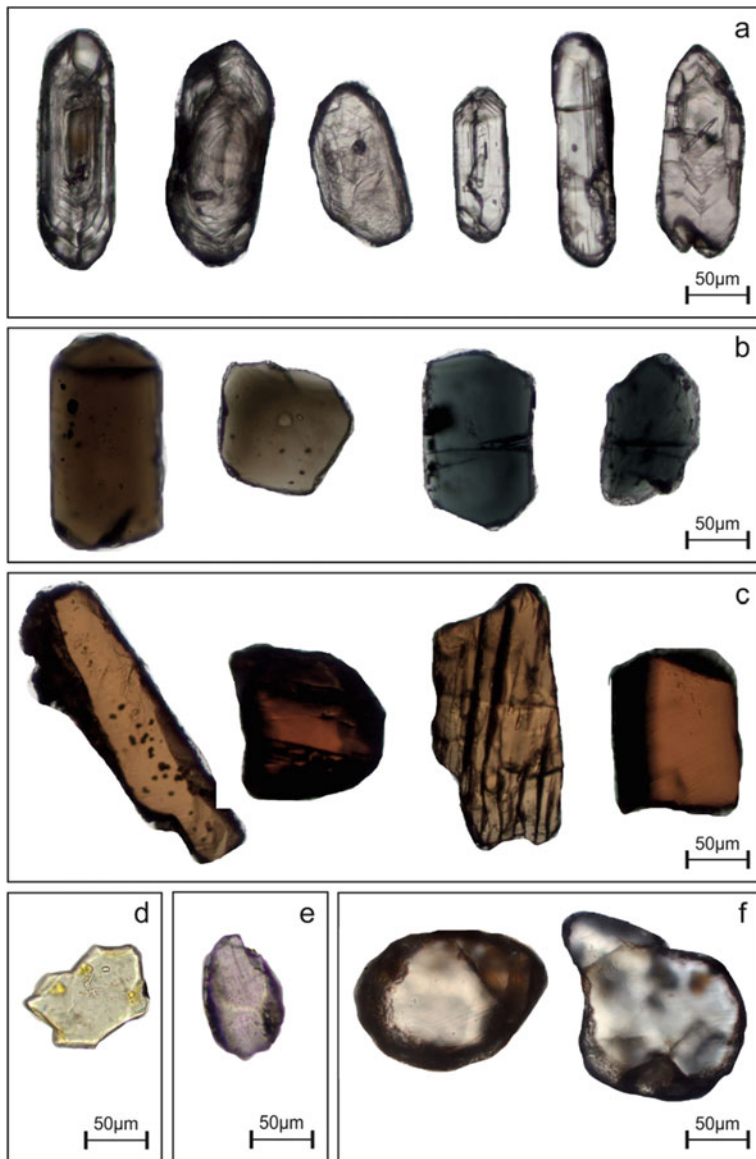


Fig. 2 Photomicrographs of transparent heavy minerals separated from sandstones (ppl)—zircon (a), tourmaline (b), rutile (c), epidote (d), apatite (e) and monazite (f)

4.2 Geochemistry

4.2.1 Major Oxides

The samples of the Jhuran Formation exhibit the lowest concentration of SiO₂ (av. 56.45%), while the samples of the Bhuj Formation show the highest concentration (av. 65.21%) (Tables 1, 2, 3 and 4). Most of the Bhuj Formation samples exhibit higher SiO₂ concentrations than the PAAS (62.80%; cf. Taylor and McLennan 1985). Al₂O₃ is the second most abundant oxide in the analysed samples. Samples of Jhumara (av. 18.98%) and Jhuran (av. 21.04%) formations exhibit average Al₂O₃ concentrations higher than the PAAS (18.90%). Samples of Jhurio (av. 11.72%) and Bhuj (av. 16.37%) formations exhibit lower concentrations than the PAAS. Samples of the Jhurio Formation exhibit the highest Fe₂O₃ content (av. 7.10%). The samples of Jhurio (av. 7.57%) and Jhumara (av. 2.23%) formations exhibit CaO concentration higher than that of the PAAS (1.30%). The samples of Jhurio, Jhumara, Jhuran and Bhuj formations exhibit average Na₂O concentrations of 0.52%, 0.39%, 0.43% and 0.34%, respectively. All the analysed samples show K₂O concentration lower than that of the PAAS (3.70%). The samples of Jhurio, Jhumara, Jhuran and Bhuj formations show average TiO₂ concentration of 0.72%, 1.23%, 1.17% and 1.09%, respectively.

Table 1 Major oxide concentration in shale samples of the Jhurio Formation

Major oxides	KU1	KU2	KU3	KU4	KU5	Avg.
SiO ₂	56.47	67.59	66.04	54.26	51.07	59.09
TiO ₂	0.46	0.72	0.58	0.81	1.04	0.72
Al ₂ O ₃	7.69	10.74	9.11	14.85	16.23	11.72
Fe ₂ O ₃	7.69	6.28	7.44	7.57	6.54	7.10
MnO	0.02	0.03	0.02	0.04	0.04	0.03
MgO	1.13	1.13	1.07	2.51	1.68	1.50
CaO	11.74	5.57	4.80	8.89	6.83	7.57
Na ₂ O	0.54	0.58	0.61	0.43	0.45	0.52
K ₂ O	2.44	2.89	2.77	2.66	2.00	2.55
P ₂ O ₅	0.03	0.03	0.03	0.13	0.07	0.06
LOI	12.85	5.17	8.16	6.33	14.94	9.49
Total	101.05	100.74	100.61	98.48	100.89	100.35
K ₂ O/Na ₂ O	4.56	4.97	4.56	6.18	4.45	4.94
SiO ₂ /Al ₂ O ₃	7.35	6.29	7.25	3.65	3.15	5.54
CIA	63.61	68.03	64.52	77.57	81.65	71.08
PIA	74.15	79.90	75.28	89.43	90.47	81.85
CIW	81.37	84.87	81.96	91.30	91.64	86.23
ICV	1.66	1.20	1.45	1.11	0.83	1.25

Table 2 Major oxide concentration in shale samples of the Jhumara Formation

Major oxides	KM1	KM2	KM3	KM4	KM5	KM6	KM7	KM8	KM9
SiO ₂	54.93	55.71	59.12	57.11	56.42	61.48	53.88	57.98	59.03
TiO ₂	1.20	1.20	1.21	1.34	1.49	1.05	1.26	1.15	0.88
Al ₂ O ₃	23.52	20.72	19.64	21.02	23.48	12.13	19.83	16.54	10.04
Fe ₂ O ₃	3.59	4.91	4.97	4.63	2.82	5.71	6.16	5.30	3.19
MnO	0.03	0.05	0.05	0.03	0.01	0.05	0.03	0.01	0.06
MgO	0.94	1.19	1.17	1.86	0.98	0.74	1.35	0.79	0.59
CaO	0.23	0.41	0.38	1.44	0.36	5.98	1.31	3.11	9.62
Na ₂ O	0.19	0.27	0.29	0.25	0.09	0.16	0.51	0.24	0.09
K ₂ O	2.18	2.20	2.38	2.65	2.27	2.51	2.63	3.49	2.49
P ₂ O ₅	0.07	0.18	0.13	0.05	0.09	0.03	0.04	0.04	0.03
LOI	13.20	14.27	12.20	11.29	12.53	10.49	12.42	11.27	12.91
Total	100.08	101.10	101.54	101.65	100.55	100.33	99.43	99.93	98.93
K ₂ O/Na ₂ O	11.36	8.30	8.21	10.67	24.32	15.89	5.12	14.52	26.82
SiO ₂ /Al ₂ O ₃	2.34	2.69	3.01	2.72	2.40	5.07	2.72	3.51	5.88
CIA	88.71	86.44	84.77	85.10	89.46	78.93	81.39	78.38	76.99
PIA	97.10	95.46	94.71	95.70	98.56	94.77	90.96	94.18	96.01
CIW	97.39	95.96	95.37	96.26	98.71	95.89	92.15	95.44	97.05
ICV	0.39	0.53	0.57	0.62	0.38	0.84	0.68	0.69	0.77
Major oxides	KM10	KM11	KM12	KM13	KM14	KM15	KM16	KM17	Avg.
SiO ₂	56.18	58.18	56.63	57.28	56.48	58.50	56.87	56.02	57.16
TiO ₂	1.22	1.27	1.36	1.34	1.32	1.38	1.31	0.97	1.23
Al ₂ O ₃	21.90	17.23	20.88	20.61	18.73	21.81	19.93	14.62	18.98
Fe ₂ O ₃	4.97	4.59	6.42	5.20	5.06	3.13	6.32	2.95	4.70
MnO	0.05	0.03	0.02	0.02	0.02	0.01	0.03	0.01	0.03
MgO	1.20	1.84	1.50	1.42	1.42	1.37	1.69	0.98	1.24
CaO	0.39	1.73	0.61	0.70	2.25	0.43	0.73	8.31	2.23
Na ₂ O	0.50	0.92	0.45	0.51	0.46	0.67	0.42	0.60	0.39
K ₂ O	2.19	2.42	2.61	2.52	2.42	2.69	2.74	2.08	2.50
P ₂ O ₅	0.15	0.04	0.05	0.07	0.04	0.07	0.05	0.04	0.07
LOI	12.70	11.58	10.85	10.90	10.70	11.42	11.41	13.58	11.98
Total	101.46	99.82	101.38	100.57	98.91	101.46	101.48	100.15	100.51
K ₂ O/Na ₂ O	4.36	2.62	5.85	4.93	5.28	4.05	6.55	3.49	9.55
SiO ₂ /Al ₂ O ₃	2.57	3.38	2.71	2.78	3.02	2.68	2.85	3.83	3.18
CIA	84.84	75.30	82.94	82.41	81.92	81.97	82.09	77.61	82.31
PIA	92.68	82.80	92.48	91.43	91.43	90.94	92.48	86.29	92.82
CIW	93.42	85.02	93.43	92.47	92.54	92.05	93.53	88.16	93.81

(continued)

Table 2 (continued)

Major oxides	KM10	KM11	KM12	KM13	KM14	KM15	KM16	KM17	Avg.
ICV	0.54	0.86	0.67	0.63	0.68	0.55	0.72	0.67	0.64

4.2.2 Trace Elements

The average Sc concentration (16.6 ppm) of samples of the Jhumara Formation is comparable to the PAAS (16.0 ppm; cf. Taylor and McLennan 1985) (Tables 5, 6, 7 and 8). The average Sc content of the samples of Jhurio, Jhuran and Bhuj formations are 12.8 ppm, 13.5 ppm and 13.9 ppm, respectively. The average Zr content (177.7 ppm) of samples of Jhurio Formation is lower than the PAAS (210.0 ppm). While samples of Jhurio (av. 151.6 ppm) and Jhumara (av. 155.2 ppm) formations show V contents similar to the PAAS (150.0 ppm), the same in Jhuran (av. 125.5 ppm) and Bhuj (av. 99.6 ppm) formations exhibits lower contents than the PAAS. The average Ni content of samples of Jhurio, Jhumara, Jhuran and Bhuj formations is lower than the PAAS (55 ppm). Samples of the Bhuj Formation show higher contents of Th and Co compared to other formations. However, the Co content in the analysed samples is lesser than the PAAS (23 ppm).

4.2.3 Rare Earth Element

The average contents of the total rare earth element (\sum REE) of Jhurio, Jhumara, Jhuran and Bhuj formations are 121 ppm, 195 ppm, 255 ppm and 256 ppm, respectively (Tables 5, 6, 7 and 8). The chondrite-normalised REE data (cf. Boynton 1983) exhibit patterns similar to those of NASC (North American Shale Composite) and PAAS (Post Archean average Australian Shale) (cf. Haskin et al. 1968; Nance and Taylor 1976; Sun and McDonough 1989).

5 Discussion

5.1 Composition of Source Rocks

Subangular grains of heavy minerals like garnet and rutile indicate nearby source rocks and/or first-cycle input while rounded to subrounded grains of ultra-stable heavy minerals like zircon and tourmaline suggest longer transportation of grains and/or recycling processes from preexisting clastic rocks (Fig. 2). The occurrence of abraded quartz overgrowths on detrital cores of quartz in these sandstones suggests the polycyclic nature (Chaudhuri et al. 2020a, b). The presence of heavy minerals with insignificant corrosion features (e.g. Andò et al. 2012) indicates the shallow

Table 3 Major oxide concentration in shale samples of the Jhuran Formation

Major oxides	KN1	KN2	KN3	KN4	KN5	KN6	KN7	KN8	KN9	KN10
SiO ₂	57.55	57.11	56.60	50.15	55.43	55.61	54.55	52.14	54.79	52.30
TiO ₂	1.14	1.14	1.11	1.05	1.07	1.03	0.99	1.13	1.02	1.01
Al ₂ O ₃	20.64	20.06	18.90	20.16	20.28	19.80	19.78	21.78	19.28	18.85
Fe ₂ O ₃	4.93	6.35	6.70	6.91	5.83	5.26	7.17	6.19	7.23	10.54
MnO	0.04	0.06	0.07	0.10	0.04	0.04	0.05	0.05	0.07	0.07
MgO	1.18	1.23	1.27	1.79	1.41	1.26	1.38	1.47	1.69	1.38
CaO	0.63	0.72	0.67	1.18	0.70	0.69	0.97	0.97	0.97	0.50
Na ₂ O	0.48	0.45	0.47	0.45	0.56	0.50	0.51	0.48	0.43	0.36
K ₂ O	2.54	2.59	2.32	2.24	2.41	2.39	2.20	2.16	2.37	2.16
P ₂ O ₅	0.14	0.13	0.10	0.16	0.15	0.18	0.13	0.12	0.14	0.10
LOI	12.00	12.79	12.89	14.38	13.98	13.39	13.89	15.51	13.01	12.40
TOTAL	101.27	102.63	101.11	98.57	101.86	100.16	101.61	101.99	101.00	99.68
K ₂ O/Na ₂ O	5.31	5.78	4.94	4.99	4.33	4.77	4.35	4.54	5.56	5.96
SiO ₂ /Al ₂ O ₃	2.79	2.85	2.99	2.49	2.73	2.81	2.76	2.39	2.84	2.77
CIA	82.67	82.40	82.33	83.78	82.02	82.38	83.04	84.79	82.92	84.25
PIA	91.90	92.11	91.38	92.31	90.60	91.26	91.29	92.55	92.26	93.28
CIW	92.91	93.14	92.44	93.17	91.71	92.32	92.25	93.29	93.22	94.06
ICV	0.58	0.65	0.69	0.71	0.65	0.61	0.68	0.60	0.74	0.80
Major oxides	KN11	KN12	KN13	KN14	KN15	KN16	KN17	KN18	KN19	KN20
SiO ₂	62.81	56.96	56.18	52.22	48.40	50.13	52.58	57.84	61.41	56.02
TiO ₂	0.91	1.07	1.07	1.06	0.96	0.98	0.97	1.04	1.06	1.06
Al ₂ O ₃	18.62	20.18	20.76	20.17	18.79	19.74	17.36	19.45	18.21	19.25
Fe ₂ O ₃	3.43	5.90	5.31	5.17	7.34	5.66	7.00	5.18	4.88	5.24
MnO	0.03	0.04	0.04	0.04	0.07	0.04	0.06	0.04	0.05	0.05
MgO	0.88	1.26	1.38	1.53	1.96	1.30	1.32	1.37	1.41	1.40
CaO	0.48	0.57	0.61	0.52	1.63	0.57	0.92	0.87	0.91	0.83
Na ₂ O	0.52	0.46	0.63	0.81	0.48	0.41	0.55	0.48	0.73	0.62
K ₂ O	2.55	2.55	2.55	2.41	2.21	2.27	2.30	2.62	2.82	2.65
P ₂ O ₅	0.07	0.11	0.12	0.11	0.71	0.13	0.11	0.11	0.12	0.14
LOI	8.92	12.84	13.27	15.03	17.39	16.74	16.97	13.16	8.96	11.27
Total	99.23	101.94	101.93	99.05	99.94	97.97	100.13	102.15	100.56	98.53
K ₂ O/Na ₂ O	4.87	5.52	4.05	2.98	4.63	5.59	4.14	5.47	3.89	4.25
SiO ₂ /Al ₂ O ₃	3.37	2.82	2.71	2.59	2.58	2.54	3.03	2.97	3.37	2.91
CIA	80.62	82.52	81.12	80.55	82.61	83.87	80.10	81.54	77.02	79.63
PIA	90.21	91.99	89.68	88.58	91.28	92.82	89.07	91.35	86.41	88.86
CIW	91.54	93.01	90.93	89.90	92.30	93.66	90.48	92.52	88.42	90.36

(continued)

Table 3 (continued)

Major oxides	KN11	KN12	KN13	KN14	KN15	KN16	KN17	KN18	KN19	KN20
ICV	0.54	0.63	0.63	0.67	0.79	0.61	0.77	0.65	0.74	0.69
Major oxides	KN21	KN22	KN23	KN24	KN25	KN26	KN27	KN28	KN29	KN30
SiO ₂	53.13	54.05	53.61	53.20	59.19	54.79	55.07	55.08	52.97	54.06
TiO ₂	1.07	1.09	1.16	1.02	1.01	1.26	1.28	1.27	1.31	1.31
Al ₂ O ₃	19.29	20.25	20.97	17.44	18.98	25.20	25.15	24.89	26.28	25.80
Fe ₂ O ₃	7.09	5.68	5.21	7.78	5.18	2.63	2.54	2.80	2.26	3.01
MnO	0.07	0.06	0.04	0.05	0.05	0.02	0.02	0.02	0.01	0.02
MgO	1.44	1.35	1.39	1.35	1.38	0.79	0.93	0.92	0.89	0.84
CaO	0.48	0.68	0.42	0.85	1.04	0.50	0.65	0.55	0.46	0.35
Na ₂ O	0.53	0.62	0.59	0.59	0.51	0.18	0.30	0.31	0.29	0.30
K ₂ O	2.41	2.60	2.59	2.32	2.65	1.88	1.94	1.85	1.64	1.64
P ₂ O ₅	0.13	0.18	0.15	0.09	0.12	0.08	0.07	0.08	0.07	0.08
LOI	12.58	12.47	13.00	14.92	11.58	13.10	13.53	13.84	15.66	14.16
Total	98.21	99.03	99.12	99.60	101.69	100.42	101.48	101.62	101.85	101.56
K ₂ O/Na ₂ O	4.56	4.21	4.42	3.91	5.24	10.34	6.52	5.89	5.75	5.49
SiO ₂ /Al ₂ O ₃	2.75	2.67	2.56	3.05	3.12	2.17	2.19	2.21	2.02	2.10
CIA	81.59	80.66	82.26	79.61	80.72	90.53	89.09	89.11	90.64	90.36
PIA	90.55	89.54	91.34	88.42	90.64	97.48	95.92	95.67	96.31	96.08
CIW	91.72	90.86	92.40	89.92	91.94	97.68	96.25	96.01	96.55	96.34
ICV	0.72	0.66	0.62	0.81	0.67	0.32	0.35	0.35	0.31	0.33
Major oxides	KN31	KN32	KN33	KN34	KN35	KN36	KN37	KN38	KN39	KN40
SiO ₂	55.71	56.85	55.27	55.69	56.13	52.90	56.93	56.61	57.68	58.33
TiO ₂	1.25	1.35	1.34	1.37	1.27	1.27	1.24	1.32	1.29	1.18
Al ₂ O ₃	22.81	23.43	23.62	23.96	24.99	23.95	21.77	23.36	22.22	17.97
Fe ₂ O ₃	3.17	3.18	2.31	2.52	2.86	3.04	4.71	3.40	3.99	6.26
MnO	0.03	0.02	0.02	0.02	0.02	0.03	0.03	0.03	0.03	0.02
MgO	0.95	0.86	0.95	0.94	0.75	1.14	0.99	1.12	0.94	0.82
CaO	0.91	0.39	0.36	0.57	0.44	0.98	0.56	1.06	0.38	2.90
Na ₂ O	0.32	0.34	0.40	0.43	0.32	0.49	0.28	0.41	0.40	0.40
K ₂ O	1.87	1.92	1.86	1.96	1.73	1.94	2.00	1.96	2.22	1.75
P ₂ O ₅	0.08	0.08	0.09	0.08	0.07	0.08	0.07	0.07	0.09	0.07
LOI	13.11	13.13	13.93	13.69	12.74	13.73	13.52	12.05	12.43	11.21
Total	100.20	101.56	100.16	101.23	101.31	99.54	102.10	101.38	101.65	100.91
K ₂ O/Na ₂ O	5.80	5.59	4.61	4.55	5.43	3.95	7.07	4.77	5.57	4.38
SiO ₂ /Al ₂ O ₃	2.44	2.43	2.34	2.32	2.25	2.21	2.61	2.42	2.60	3.25

(continued)

Table 3 (continued)

Major oxides	KN31	KN32	KN33	KN34	KN35	KN36	KN37	KN38	KN39	KN40
CIA	88.07	87.97	87.61	87.12	89.55	86.58	87.53	87.05	85.70	81.08
PIA	95.14	94.98	94.22	93.90	95.67	93.12	95.46	94.01	93.80	91.98
CIW	95.55	95.41	94.68	94.41	95.98	93.68	95.89	94.53	94.44	93.18
ICV	0.40	0.39	0.38	0.39	0.33	0.43	0.47	0.44	0.46	0.66
Major oxides	KN41	KN42	KN43	KN44	KN45	KN46	KN47	KN48	KN49	KN50
SiO ₂	63.31	59.52	60.36	62.87	59.20	59.97	57.60	55.47	56.37	56.80
TiO ₂	1.29	1.34	1.32	1.34	1.32	1.39	1.30	1.42	1.18	1.16
Al ₂ O ₃	19.17	20.66	22.05	21.63	20.72	21.55	21.97	21.85	21.93	20.99
Fe ₂ O ₃	2.37	2.37	2.67	2.18	3.03	3.43	1.37	4.56	1.36	5.55
MnO	0.01	0.01	0.01	0.01	0.01	0.01	1.81	0.02	1.96	0.04
MgO	1.03	0.97	0.89	0.73	1.02	1.07	1.56	1.02	1.39	1.45
CaO	0.64	1.29	0.65	0.33	0.96	0.60	1.03	1.17	1.06	0.22
Na ₂ O	0.59	0.59	0.17	0.39	0.34	0.30	0.35	0.50	0.23	0.38
K ₂ O	2.00	1.99	1.98	1.99	1.99	2.12	2.32	1.89	2.17	2.48
P ₂ O ₅	0.07	0.07	0.09	0.08	0.08	0.08	0.02	0.09	0.02	0.08
LOI	9.99	10.98	10.35	9.71	10.84	10.69	12.59	13.51	14.51	12.91
Total	100.47	99.79	100.54	101.26	99.51	101.21	101.92	101.50	102.18	102.06
K ₂ O/Na ₂ O	3.39	3.37	11.65	5.10	5.85	7.07	6.63	3.78	9.43	6.53
SiO ₂ /Al ₂ O ₃	3.30	2.88	2.74	2.91	2.86	2.78	2.62	2.54	2.57	2.71
CIA	78.56	79.85	85.25	82.73	82.51	82.81	81.56	82.13	83.52	80.44
PIA	89.11	89.96	97.11	93.67	93.98	94.82	94.04	91.93	96.04	94.29
CIW	90.81	91.41	97.53	94.57	94.88	95.62	95.02	93.00	96.66	95.34
ICV	0.57	0.53	0.43	0.44	0.51	0.52	0.64	0.55	0.59	0.66
Major oxides	KN51	KN52	KN53	KN54	KN55	Avg.				
SiO ₂	58.26	59.20	59.53	61.12	61.37	56.35				
TiO ₂	1.12	1.16	1.14	1.09	1.09	1.17				
Al ₂ O ₃	20.36	20.74	20.97	19.14	19.18	21.04				
Fe ₂ O ₃	4.22	4.88	4.50	3.85	3.88	4.58				
MnO	0.04	0.02	0.02	0.02	0.02	0.10				
MgO	1.44	1.55	1.40	1.22	1.22	1.21				
CaO	0.22	0.27	0.26	0.16	0.15	0.72				
Na ₂ O	0.40	0.55	0.26	0.25	0.18	0.43				
K ₂ O	2.92	2.55	2.80	2.92	2.93	2.26				
P ₂ O ₅	0.07	0.06	0.07	0.06	0.06	0.11				
LOI	12.86	9.29	10.41	9.93	9.95	12.76				
Total	101.91	100.27	101.36	99.76	100.03	100.72				

(continued)

Table 3 (continued)

Major oxides	KN51	KN52	KN53	KN54	KN55	Avg.
K ₂ O/Na ₂ O	7.30	4.64	10.77	11.68	16.28	5.77
SiO ₂ /Al ₂ O ₃	2.86	2.85	2.84	3.19	3.20	2.71
CIA	77.65	78.77	79.34	77.66	78.07	83.16
PIA	93.63	92.22	95.03	95.33	96.19	92.74
CIW	95.06	93.70	96.08	96.46	97.12	93.68
ICV	0.67	0.68	0.64	0.65	0.65	0.58

burial of sediments (e.g. Morton 1984). Heavy minerals such as epidote display a limit of persistence between 600 and 1100 m depth (e.g. Morton 1984), or between 600 and 3000 m (e.g. McBride 1985) as burial diagenesis proceeds. The geochemical analysis by Arora et al. (2017) indicated the low maturity of organic matters within the Mesozoic succession in Mainland Kutch, except near a few dike intrusions. The heavy mineral assemblage, therefore, corroborates the shallow burial nature of sediments.

In a cross-plot of TiO₂ and Al₂O₃, apart from a few samples of Jhumara and Bhuj formations which plot closer to the basalt line, data of all four formations plot in the granite + basalt field (cf. McLennan et al. 1979; Schieber 1992) (Fig. 3). In a cross-plot of TiO₂ and Zr of Hayashi et al. (1997), most of the samples plot in the field for intermediate igneous rocks. A few samples of all the formations plot in the field for felsic igneous rocks (Fig. 4). In a cross-plot of Th versus Sc of Cullers (2002), most samples of Jhuran and Bhuj formations and nearly half of the data Jhurio and Jhumara formations bear felsic signature (Fig. 5). A few samples of Jhuran and Bhuj formations and the majority of those of Jhurio and Jhumara formations plot within the intermediate field. In a cross-plot of Th/Co versus La/Sc of Cullers (2002), all data cluster near the silicic field (Fig. 6). Most data cluster near the field marked for felsic rocks in a triangular plot of V-Ni-Th × 10 of Bracciali et al. (2007) (Fig. 7). Samples of the Jhuran and Bhuj formations plot close to the Th apex. Data of Jhurio and Jhumara formations and a few of those of the Jhuran Formation plot relatively closer to the V-Ni join. Samples of all four formations exhibit low La/Th ratios ranging from 1.59 to 3.01 (Tables 5, 6, 7 and 8). Samples of Jhurio, Jhumara, Jhuran and Bhuj formations show broadly overlapping chondrite-normalized REE patterns, with prominent LREE enrichment and negative europium anomaly (Fig. 8). These patterns are similar to those of NASC and PAAS samples. The samples of Jhuran and Bhuj formations exhibit the highest REE concentrations. All samples of Jhurio, Jhumara, Jhuran and Bhuj formations exhibit negative Eu anomalies (Eu/Eu* = Eu/(√(Sm_N × Nd_N)), with averages of 0.66, 0.65, 0.65 and 0.55 respectively.

The presence of both rounded, as well as angular varieties of heavy minerals, indicate the presence of multiple source rocks. Chaudhuri et al. (2018, 2020a, b) report the dominance of arkoses in the sandstones of the Jhurio, Jhumara, Jhuran and Bhuj formations suggesting a significant clastic supply from felsic source rocks. The abundance of arkose, the relationship between TiO₂ and Al₂O₃, Th/Co and La/Sc

Table 4 Major oxide concentration in shale samples of the Bhuj Formation

Major oxides	KB1	KB2	KB3	KB4	KB5	KB6	KB7	KB8	KB9	KB10
SiO ₂	58.85	54.54	54.61	57.67	65.69	67.55	66.99	65.64	75.75	76.76
TiO ₂	1.22	1.11	1.05	1.06	1.08	1.10	1.10	1.17	0.91	0.82
Al ₂ O ₃	22.77	21.23	21.14	16.73	16.40	17.13	16.44	18.03	10.80	11.21
Fe ₂ O ₃	2.83	5.85	6.94	7.90	3.97	3.69	4.13	3.29	4.92	3.74
MnO	0.09	0.07	0.08	0.03	0.05	0.05	0.04	0.06	0.05	0.10
MgO	1.11	1.37	1.28	1.41	0.72	0.68	0.68	0.84	0.39	0.35
CaO	0.35	0.42	0.28	0.33	0.22	0.15	0.20	0.11	0.07	0.09
Na ₂ O	0.18	0.14	0.20	0.10	0.28	0.29	0.30	0.32	0.21	0.44
K ₂ O	2.76	2.41	2.38	2.86	1.99	2.09	2.01	2.16	2.93	3.19
P ₂ O ₅	0.07	0.07	0.06	0.07	0.05	0.05	0.05	0.06	0.04	0.04
LOI	11.01	12.05	11.59	10.78	9.16	8.96	9.08	9.80	4.32	3.52
Total	101.25	99.26	99.61	98.95	99.61	101.75	101.01	101.47	100.40	100.25
K ₂ O/Na ₂ O	15.32	17.43	12.11	28.65	7.12	7.29	6.78	6.76	13.90	7.23
SiO ₂ /Al ₂ O ₃	2.58	2.57	2.58	3.45	4.01	3.94	4.08	3.64	7.01	6.85
CIA	86.42	87.40	86.78	82.99	84.47	85.03	84.48	85.48	74.71	72.10
PIA	97.09	97.62	96.64	97.64	94.28	95.19	94.40	95.61	94.06	89.74
CIW	97.46	97.91	97.03	98.07	94.99	95.80	95.10	96.16	95.73	92.66
ICV	0.43	0.55	0.58	0.80	0.54	0.50	0.54	0.49	0.83	0.79
Major oxides	KB11	KB12	KB13	KB14	KB15	KB16	KB17	KB18	Avg.	
SiO ₂	66.36	74.17	67.03	68.68	61.67	56.91	65.63	69.24	65.21	
TiO ₂	0.88	1.21	0.97	0.98	1.45	1.30	1.06	1.22	1.09	
Al ₂ O ₃	8.89	15.41	15.95	15.50	16.82	20.03	12.66	17.45	16.37	
Fe ₂ O ₃	7.28	1.03	4.58	2.59	1.33	1.58	10.41	0.87	4.27	
MnO	0.05	0.01	0.34	0.02	0.01	0.01	0.02	0.01	0.06	
MgO	0.56	0.49	0.81	0.77	0.45	0.59	0.52	0.43	0.75	
CaO	5.35	0.12	0.29	0.39	0.05	0.07	0.08	0.10	0.48	
Na ₂ O	0.58	0.91	0.21	0.30	0.12	0.16	0.48	0.84	0.34	
K ₂ O	2.65	2.12	3.66	3.63	1.52	1.65	3.44	3.21	2.59	
P ₂ O ₅	0.05	0.04	0.06	0.04	0.03	0.04	0.07	0.05	0.05	
LOI	7.76	6.25	6.65	7.02	18.19	17.98	5.58	7.59	9.29	
Total	100.42	101.75	100.55	99.92	101.64	100.31	99.94	101.01	100.51	
K ₂ O/Na ₂ O	4.58	2.31	17.06	12.23	12.38	10.57	7.22	3.82	10.71	
SiO ₂ /Al ₂ O ₃	7.47	4.81	4.20	4.43	3.67	2.84	5.18	3.97	4.29	
CIA	65.02	79.37	77.36	75.94	89.61	90.23	73.15	77.57	81.01	
PIA	75.92	88.44	94.44	92.21	98.06	97.96	90.64	89.92	93.32	
CIW	82.33	89.99	95.76	94.07	98.24	98.14	93.21	91.76	94.69	

(continued)

Table 4 (continued)

Major oxides	KB11	KB12	KB13	KB14	KB15	KB16	KB17	KB18	Avg.
ICV	1.36	0.48	0.71	0.63	0.34	0.32	1.10	0.47	0.64

and V-Ni-Th support the dominance of felsic source rocks (Cullers 2002; López et al. 2005; Bracciali et al. 2007; Etemad-Saeed et al. 2011; Amendola et al. 2016; Armstrong-Altrin et al. 2017) (Figs. 3, 6 and 7). The relationship between TiO₂ and Al₂O₃ suggests the input from mafic sources in these sediments (Fig. 3). The intermediate igneous source rock composition, indicated by the relationship between TiO₂ and Zr contents, possibly indicates a mixing of sediments from felsic and mafic igneous rocks (Fig. 4). The relationship between Th versus Sc supports the mixing of sediments from mafic and felsic igneous rocks (Fig. 5). The fields for Jhurio and Jhumara formations plot closer to the V-Ni join in the triangular plot of V-Ni-Th and thereby corroborate the mafic input in these formations (Fig. 7). Low La/Th ratios support the predominant felsic source of sediments (Floyd and Leveridge 1987; Gu et al. 2002; Etemad-Saeed et al. 2011; Zhu et al. 2011; Yan et al. 2012). The LREE enrichment, the resemblance of the chondrite-normalized REE patterns with those of NASC and PAAS and negative Eu anomalies endorse the dominance of felsic source rocks in sediments (Fig. 8) (Kasanzu et al. 2008; Wani and Mondal 2011; Wang et al. 2015; Löwen et al. 2018; Chaudhuri et al. 2020a).

5.2 Weathering and Recycling

The degree of chemical weathering of source rocks is calculated from the chemical index of alteration (CIA) (Nesbitt and Young 1982) using the following formula (in molecular proportions)

$$\text{CIA} = [n(\text{Al}_2\text{O}_3)/(n(\text{Al}_2\text{O}_3) + n(\text{CaO}) * + n(\text{Na}_2\text{O}) + n(\text{K}_2\text{O}))] \times 100$$

The CaO content associated with calcite, dolomite and apatite is corrected to find CaO* (CaO in silicates). Further, McLennan (1993) suggested if $n(\text{CaO}') < n(\text{Na}_2\text{O})$, $n(\text{CaO}^*) = n(\text{CaO}')$ else, $n(\text{CaO}^*) = n(\text{Na}_2\text{O})$ where $n(\text{CaO}') = n(\text{CaO}) - 10 \times n(\text{P}_2\text{O}_5)/3$. Samples of Jhurio, Jhumara, Jhuran and Bhuj formations exhibit average CIA values of 71%, 82%, 83% and 81%, respectively. Two other indices used to study the extent of weathering and alteration are the plagioclase index of alteration (PIA) and the chemical index of weathering (CIW). K-metasomatism during diagenesis may modify the values of CIA. Therefore, PIA and CIW are used for unbiased estimation of weathering conditions (Harnois 1988; Fedo et al. 1995).

$$\begin{aligned} \text{PIA} &= [(\text{Al}_2\text{O}_3 - \text{K}_2\text{O})/(\text{Al}_2\text{O}_3 - \text{K}_2\text{O}) + \text{CaO} * + \text{Na}_2\text{O}] \times 100 \\ \text{CIW} &= [\text{Al}_2\text{O}_3/(\text{Al}_2\text{O}_3 + \text{CaO} * + \text{Na}_2\text{O})] \times 100 \end{aligned}$$

Table 5 Trace element concentration in shale samples from Jhurio Formation

Elements	KU1	KU2	KU3	KU4	KU5	Avg.
Sc	7.3	9.5	10.1	16.9	20.3	12.8
V	121.2	117.3	192.7	127.4	199.6	151.6
Cr	115.5	153.3	148.7	89.6	118.4	125.1
Co	9.1	16.3	11.9	13.6	13.9	13.0
Ni	30.9	36.6	42.1	27.2	39.4	35.2
Cu	17.0	22.3	21.4	29.3	33.5	24.7
Zn	31.8	44.4	86.0	43.2	51.0	51.3
Ga	9.3	12.8	12.0	13.7	20.7	13.7
Rb	63.0	86.1	79.9	118.0	100.6	89.5
Sr	254.6	159.8	240.0	619.2	168.9	288.5
Y	9.4	12.7	11.2	24.0	20.0	15.4
Zr	143.0	219.7	219.9	125.6	180.1	177.7
Nb	8.4	12.9	9.2	14.6	16.8	12.4
Cs	1.5	2.4	2.0	5.7	6.7	3.7
Ba	627.9	761.0	810.7	426.3	152.0	555.6
La	16.6	22.9	21.7	35.7	35.3	26.4
Ce	33.9	48.8	49.8	58.9	64.1	51.1
Pr	3.9	5.1	5.2	7.6	7.5	5.8
Nd	13.7	17.8	18.0	27.9	26.4	20.8
Sm	2.6	3.1	3.2	5.5	5.0	3.9
Eu	0.6	0.7	0.7	1.1	1.0	0.8
Gd	2.2	2.5	2.4	4.9	4.2	3.3
Tb	0.4	0.5	0.4	0.8	0.8	0.6
Dy	1.9	2.5	2.2	4.3	4.1	3.0
Ho	0.4	0.5	0.5	0.9	0.9	0.7
Er	1.2	1.6	1.5	2.6	2.6	1.9
Tm	0.2	0.2	0.2	0.4	0.4	0.3
Yb	1.2	1.8	1.6	2.5	2.7	2.0
Lu	0.2	0.3	0.3	0.4	0.4	0.3
Hf	4.2	6.4	6.5	3.8	5.6	5.3
Ta	0.7	0.9	0.3	1.0	0.7	0.7
Pb	14.2	17.2	32.2	13.6	18.6	19.2
Th	9.2	11.6	13.6	12.7	15.6	12.5
U	1.3	2.0	2.3	1.7	2.0	1.9
La/Th	1.8	2.0	1.6	2.8	2.3	2.1
La/Sc	2.3	2.4	2.1	2.1	1.7	2.1

(continued)

Table 5 (continued)

Elements	KU1	KU2	KU3	KU4	KU5	Avg.
Th/Co	1.0	0.7	1.1	0.9	1.1	1.0
Th/Sc	1.3	1.2	1.3	0.8	0.8	1.1
\sum REE	78.8	108.3	107.6	153.5	155.4	120.7
(Gd _N /Yb _N)	1.4	1.2	1.2	1.6	1.3	1.3
Eu/Eu*	1.3	2.1	1.8	2.8	3.3	2.3

Samples of Jhurio, Jhumara, Jhuran and Bhuj formations exhibit average PIA values of 82%, 93%, 93% and 93% respectively. The samples exhibit average CIW values of 86%, 94%, 94% and 95%, respectively.

The index of compositional variability (ICV) proposed by Cox et al. (1995) is defined as follows.

$$\text{ICV} = (n(\text{Fe}_2\text{O}_3) + n(\text{K}_2\text{O}) + n(\text{Na}_2\text{O}) + n(\text{CaO}* \\ + n(\text{MgO}) + n(\text{MnO}) + n(\text{TiO}_2)) / n(\text{Al}_2\text{O}_3).$$

Samples of Jhurio, Jhumara, Jhuran and Bhuj formations exhibit average ICV of 1.3, 0.7, 0.6 and 0.6, respectively.

Chemical weathering and alteration of source rocks influence geochemistry and mineralogy of sedimentary rocks (Nesbitt and Young 1982; McLennan 1993; Fedo et al. 1995). Diagenesis and low-grade metamorphism lead to changes in mineralogy. However, the bulk chemical composition remains similar to that of source rock(s) (Cox et al. 1995). CIA values indicate intermediate to strong weathering for Jhurio, Jhumara, Jhuran and Bhuj formations (Fig. 9). However, a few samples of the Jhurio Formation indicate weak weathering. PIA and CIW indicate a greater degree of weathering at source than that estimated by CIA. However, all three indices show a broadly similar trend of weathering. Thus, CIA, PIA and CIW data for the studied samples indicate weak to intermediate weathering of source rocks for the Jhurio Formation. The data also indicates intermediate to strong weathering of source rocks for Jhumara, Jhuran and Bhuj formations.

Mature sediments with high clay content exhibit ICV values less than 1. It generally indicates a passive tectonic setting with recycling or intense chemical weathering of first cycle sediments (cf. Cox et al. 1995). The ICV value exceeds 1 in case of immature sediments containing a high amount of non-clay minerals. It generally indicates the first cycle deposition sourced from tectonically active regions (Cox et al. 1995; Cullers and Podkorytov 2000; Ding et al. 2016). Therefore, the average ICV values of samples of Jhumara, Jhuran and Bhuj formations suggest recycled sediments or highly weathered first cycle sediments in a passive tectonic setting (Fig. 10). However, the average ICV values of the Jhurio Formation suggest immature sediments supplied from tectonically active sediments.

Table 6 Trace element concentration in shale samples of the Jhumara Formation

Elements	KM1	KM2	KM3	KM4	KM5	KM6	KM8	KM9
Sc	14.5	15.9	13.4	13.9	11.9	11.1	18.1	7.9
V	169.9	139.9	116.0	111.7	152.2	109.1	164.7	87.2
Cr	138.9	132.5	108.9	97.3	107.3	130.0	121.3	93.8
Co	20.3	21.3	19.5	18.8	6.4	15.9	22.3	11.9
Ni	48.1	44.2	35.1	33.4	38.2	45.2	36.4	28.0
Cu	45.4	42.4	36.6	27.8	28.8	41.9	31.1	20.9
Zn	89.2	84.3	48.2	26.8	117.9	73.3	36.3	36.5
Ga	37.4	31.2	26.1	25.5	27.4	15.8	24.8	11.6
Rb	106.2	108.0	97.0	90.7	91.4	81.6	78.7	62.9
Sr	164.9	321.9	210.7	315.9	181.4	200.7	125.8	129.2
Y	22.4	27.6	21.2	27.2	8.6	19.5	25.9	13.5
Zr	255.4	312.4	272.7	233.4	188.0	384.5	272.2	246.2
Nb	29.3	27.8	24.5	23.2	24.2	18.6	26.5	15.7
Cs	8.7	6.4	5.0	5.0	7.3	3.8	7.4	2.9
Ba	303.4	466.9	480.8	445.3	142.6	458.7	257.4	351.1
La	51.3	64.0	46.1	55.9	28.2	41.2	40.9	28.6
Ce	153.0	152.1	99.4	133.0	87.0	96.8	105.9	72.1
Pr	11.6	14.5	9.3	13.0	6.0	9.3	9.5	6.7
Nd	40.6	51.5	31.3	46.9	20.2	31.9	32.9	23.3
Sm	7.7	9.6	5.5	9.1	3.4	5.9	6.3	4.3
Eu	1.4	1.9	1.1	1.9	0.6	1.0	1.3	0.8
Gd	6.0	7.5	4.7	7.4	2.3	4.7	5.3	3.4
Tb	1.0	1.2	0.8	1.1	0.4	0.8	0.9	0.5
Dy	4.9	6.1	4.4	5.8	1.9	3.9	5.2	2.8
Ho	1.0	1.2	0.9	1.1	0.4	0.8	1.1	0.5
Er	2.7	3.4	2.6	3.0	1.2	2.3	3.2	1.6
Tm	0.4	0.5	0.4	0.4	0.2	0.3	0.5	0.2
Yb	2.8	3.5	2.8	3.0	1.5	2.5	3.6	1.7
Lu	0.5	0.6	0.5	0.5	0.3	0.4	0.6	0.3
Hf	6.0	7.2	6.2	5.5	4.4	8.8	6.4	5.8
Ta	2.3	2.2	1.9	2.0	1.8	1.6	2.1	1.2
Pb	21.4	19.1	16.2	15.1	10.6	15.9	16.7	10.8
Th	25.5	23.6	19.6	18.9	12.9	17.8	17.6	12.3
U	5.4	4.1	3.5	3.5	1.9	2.8	2.4	2.0
La/Th	2.0	2.7	2.4	3.0	2.2	2.3	2.3	2.3
La/Sc	3.5	4.0	3.4	4.0	2.4	3.7	2.3	3.6

(continued)

Table 6 (continued)

Elements	KM1	KM2	KM3	KM4	KM5	KM6	KM8	KM9
Th/Co	1.3	1.1	1.0	1.0	2.0	1.1	0.8	1.0
Th/Sc	1.8	1.5	1.5	1.4	1.1	1.6	1.0	1.6
\sum REE	284.9	317.4	209.7	282.2	153.7	201.9	217.1	146.9
(Gd _N /Yb _N)	1.7	1.7	1.3	2.0	1.2	1.5	1.2	1.6
Eu/Eu*	0.6	0.7	0.7	0.7	0.7	0.6	0.7	0.6
Elements	KM11	KM12	KM13	KM14	KM15	KM16	KM17	Avg.
Sc	19.5	21.9	24.0	19.6	20.6	21.2	15.1	16.6
V	170.6	196.9	209.3	189.8	177.5	198.8	134.5	155.2
Cr	127.3	131.2	140.9	130.7	133.1	139.4	108.6	122.8
Co	19.0	20.7	20.7	20.0	7.4	23.2	6.8	17.0
Ni	39.3	44.7	46.3	43.4	35.3	47.6	29.3	39.6
Cu	62.2	40.1	41.2	39.5	23.8	40.1	18.8	36.0
Zn	56.6	44.2	38.4	49.3	24.9	54.1	25.8	53.7
Ga	22.2	27.2	29.8	24.1	27.2	25.7	17.8	24.9
Rb	110.2	122.7	133.4	112.1	131.1	130.5	96.7	103.5
Sr	107.3	119.6	108.9	100.4	145.9	105.0	206.9	169.6
Y	22.6	20.1	24.6	20.9	18.1	19.6	13.9	20.4
Zr	267.4	229.1	249.2	229.7	210.2	206.2	172.4	248.6
Nb	22.6	23.7	26.8	23.1	24.2	22.9	16.9	23.3
Cs	7.1	8.8	9.4	7.7	9.7	8.8	6.4	7.0
Ba	307.2	276.7	286.2	264.3	264.5	264.4	215.0	319.0
La	35.7	38.2	42.4	34.8	38.1	33.9	24.7	40.3
Ce	69.5	84.0	84.9	74.0	70.8	66.6	47.0	93.1
Pr	7.3	8.4	8.8	7.3	7.1	6.9	4.9	8.7
Nd	24.5	28.9	29.9	25.0	22.6	23.3	16.2	29.9
Sm	4.5	5.2	5.6	4.5	3.8	4.2	2.9	5.5
Eu	0.8	1.0	1.1	0.9	0.7	0.8	0.6	1.1
Gd	3.8	4.1	4.7	3.7	3.1	3.6	2.4	4.5
Tb	0.7	0.7	0.8	0.7	0.6	0.7	0.4	0.8
Dy	4.1	4.1	4.7	3.9	3.2	3.7	2.5	4.1
Ho	0.9	0.9	1.1	0.9	0.8	0.8	0.6	0.9
Er	2.8	2.7	3.2	2.7	2.3	2.5	1.8	2.5
Tm	0.4	0.4	0.5	0.4	0.3	0.4	0.3	0.4
Yb	3.1	2.9	3.4	2.9	2.6	2.7	2.0	2.7
Lu	0.5	0.5	0.6	0.5	0.4	0.4	0.3	0.4
Hf	7.9	6.8	7.4	6.9	6.4	6.1	5.1	6.5

(continued)

Table 6 (continued)

Elements	KM11	KM12	KM13	KM14	KM15	KM16	KM17	Avg.
Ta	1.8	2.0	2.1	1.8	1.7	1.8	1.4	1.8
Pb	26.1	34.6	23.4	23.3	19.1	22.1	13.2	19.2
Th	17.8	17.9	19.9	18.4	16.0	18.1	12.3	17.9
U	2.3	2.2	2.5	2.3	2.3	2.2	1.6	2.7
La/Th	2.0	2.1	2.1	1.9	2.4	1.9	2.0	2.2
La/Sc	1.8	1.7	1.8	1.8	1.8	1.6	1.6	2.6
Th/Co	0.9	0.9	1.0	0.9	2.2	0.8	1.8	1.2
Th/Sc	0.9	0.8	0.8	0.9	0.8	0.9	0.8	1.1
$\sum \text{REE}$	158.6	182.1	191.5	162.2	156.6	150.7	106.7	194.8
(Gd _N /Yb _N)	1.0	1.2	1.1	1.0	1.0	1.1	1.0	1.3
Eu/Eu*	0.6	0.7	0.7	0.6	0.6	0.7	0.7	0.7

5.3 Tectonic Setting

In a cross plot of SiO₂ and K₂O/Na₂O of Roser and Korsch (1986), the analysed shale samples plot in the passive continental margin field (Fig. 11). In a cross-plot of SiO₂/Al₂O₃ and K₂O/Na₂O of Maynard et al. (1982), the majority of the analysed samples exhibit passive margin signatures (Fig. 12). However, many samples of Jhurio, Jhumara and Bhuj formations plot at the margin of ACM (active continental margin) and PM (passive margin) fields. In the cross-plot of La/Th versus Hf of Floyd and Leveridge (1987), the majority of the samples Jhurio, Jhumara, Jhuran and Bhuj formations indicate passive margin source, while a few samples of all the formations occupy the field of acidic arc source (Fig. 13). Samples of Jhuran and Bhuj formations exhibit a distinctly higher concentration of Hf in comparison to those of Jhurio and Jhumara formations.

The concentration of major oxides and trace elements in samples of Jhurio, Jhumara, Jhuran and Bhuj formations indicate the predominantly passive margin setting (Figs. 11, 12 and 13). The offset of data points to the active continental margin field (Fig. 12) corresponds to the higher abundance of Al₂O₃ in most of shale samples.

5.4 Age of Source Rock

In a cross plot of Cr and Ni of Taylor and McLennan (1985), the majority of the analysed shale samples of Jhurio, Jhumara, Jhuran and Bhuj formations cluster in the field marked for post-Archean source rocks (Fig. 14). However, a few samples of the Jhuran Formation plot in the Late Archean field. Further, most samples of all the formations occupy the Post-Archean field in the Eu/Eu* versus (Gd_N/Yb_N) plot

Table 7 Trace element concentration in shale samples of the Jhuran Formation

Elements	KN1	KN2	KN3	KN4	KN5	KN6	KN7	KN8	KN9	KN10
Sc	15.0	16.1	10.4	17.3	16.2	16.3	18.9	18.6	10.3	19.7
V	132.8	109.9	90.1	87.2	139.9	129.4	123.5	158.9	95.4	148.3
Cr	125.8	105.0	77.9	91.9	141.3	130.9	117.8	136.0	91.9	109.5
Co	20.7	23.5	17.4	27.8	20.4	21.2	23.0	24.6	11.1	15.0
Ni	47.3	47.3	38.5	57.1	65.8	63.5	51.8	49.1	35.5	50.7
Cu	60.5	48.7	47.0	60.0	131.9	124.7	54.1	63.5	43.1	90.7
Zn	144.5	113.6	94.6	175.5	155.7	218.2	972.8	95.0	146.8	170.0
Ga	28.0	32.9	23.8	36.2	26.6	23.9	33.9	28.6	25.1	24.3
Rb	113.6	113.8	98.6	105.2	106.0	102.3	110.5	103.1	103.0	94.0
Sr	237.3	212.4	149.1	307.7	265.3	260.3	336.6	125.9	189.8	242.8
Y	28.8	32.4	27.7	47.3	29.2	32.8	38.3	31.6	30.6	45.6
Zr	191.6	258.9	269.3	308.4	227.9	309.8	233.9	189.8	204.2	171.3
Nb	21.2	23.7	21.6	28.6	20.7	20.4	23.0	21.2	20.5	18.7
Cs	6.7	6.0	5.0	5.4	8.0	6.2	6.5	6.1	6.1	6.5
Ba	572.3	617.6	586.7	398.2	776.1	768.3	597.0	461.1	503.0	534.6
La	72.1	64.2	72.0	61.2	99.7	88.8	71.5	53.3	58.4	61.1
Ce	138.2	116.5	133.5	113.5	195.6	165.8	137.3	98.8	108.3	116.9
Pr	19.4	16.6	17.4	15.6	27.5	22.7	19.5	13.5	14.3	17.2
Nd	69.9	59.8	60.8	67.2	97.8	82.2	72.6	47.6	51.1	64.8
Sm	11.4	9.4	10.1	11.8	15.5	14.6	12.0	8.3	8.8	12.5
Eu	2.0	1.8	1.5	2.5	3.0	2.6	2.4	1.7	1.7	2.7
Gd	10.8	8.0	8.9	12.2	14.4	13.0	10.4	7.7	8.3	11.5
Tb	1.4	1.2	1.2	1.7	1.9	1.8	1.6	1.2	1.2	2.0
Dy	7.3	6.9	6.5	7.8	10.4	9.8	8.4	7.0	6.6	11.6
Ho	1.3	1.2	1.2	1.3	1.8	1.8	1.5	1.3	1.3	2.3
Er	3.5	3.3	3.4	3.6	5.0	5.0	4.2	3.7	3.6	6.2
Tm	0.6	0.6	0.6	0.6	0.8	0.8	0.7	0.6	0.6	1.0
Yb	3.4	3.5	3.5	4.0	4.9	4.9	4.4	3.7	3.6	6.3
Lu	0.5	0.6	0.6	0.8	0.8	0.8	0.7	0.6	0.6	1.0
Hf	5.9	8.3	7.9	7.2	10.2	13.0	7.7	5.8	6.2	6.1
Ta	1.4	1.7	1.3	1.2	1.9	1.8	1.3	1.3	1.4	1.4
Pb	23.6	28.8	18.1	21.1	34.9	27.6	28.0	21.4	23.2	23.9
Th	25.4	24.2	34.0	22.6	33.1	39.9	23.8	22.8	23.4	25.0
U	3.5	3.5	4.3	2.6	4.7	5.6	3.9	3.4	3.5	3.6
La/Th	2.8	2.7	2.1	2.7	3.0	2.2	3.0	2.3	2.5	2.4
La/Sc	4.8	4.0	6.9	3.5	6.2	5.4	3.8	2.9	5.7	3.1

(continued)

Table 7 (continued)

Elements	KN1	KN2	KN3	KN4	KN5	KN6	KN7	KN8	KN9	KN10
Th/Co	1.2	1.0	2.0	0.8	1.6	1.9	1.0	0.9	2.1	1.7
Th/Sc	1.7	1.5	3.3	1.3	2.0	2.4	1.3	1.2	2.3	1.3
\sum REE	341.8	293.6	321.2	303.8	479.1	414.6	347.2	249.0	268.4	317.1
(Gd _N /Yb _N)	2.6	1.8	2.1	2.5	2.4	2.1	1.9	1.7	1.9	1.5
Eu/Eu*	0.6	0.6	0.5	0.6	0.6	0.6	0.7	0.7	0.6	0.7
Elements	KN11	KN12	KN15	KN16	KN17	KN18	KN19	KN20		
Sc	15.4	12.3	15.6	15.1	16.6	17.9	15.2	15.9		
V	134.9	76.4	145.2	106.4	116.3	118.9	121.7	120.9		
Cr	126.3	73.2	124.2	107.4	104.7	111.7	139.9	112.7		
Co	19.9	15.1	17.3	24.1	24.5	20.3	26.0	23.5		
Ni	43.0	34.6	48.0	60.1	52.4	46.1	40.8	45.9		
Cu	56.0	34.4	62.0	51.1	47.7	53.8	162.2	42.3		
Zn	128.5	64.0	149.9	88.6	86.4	80.1	64.2	71.2		
Ga	23.6	32.2	28.2	28.1	33.4	30.4	25.8	25.6		
Rb	107.0	117.7	113.8	108.1	107.5	107.5	120.8	108.0		
Sr	187.5	167.4	209.5	138.3	161.1	277.3	145.0	212.0		
Y	26.3	40.2	27.8	38.1	45.1	40.7	28.9	30.8		
Zr	205.7	287.8	156.3	234.3	223.5	244.5	312.8	285.6		
Nb	20.3	24.1	19.8	21.9	23.3	21.5	22.5	22.2		
Cs	5.5	6.5	8.4	5.7	6.3	5.6	5.6	4.6		
Ba	544.0	590.7	397.1	550.5	515.2	620.6	687.0	637.5		
La	56.8	60.3	61.2	56.4	61.9	65.3	43.8	55.1		
Ce	106.5	106.6	112.2	108.0	116.8	126.0	91.8	122.1		
Pr	14.7	15.4	15.9	16.1	17.0	18.0	9.7	12.6		
Nd	52.1	56.8	54.4	61.5	63.8	68.7	34.1	44.3		
Sm	8.5	10.1	8.0	11.4	11.7	12.6	7.0	8.6		
Eu	1.6	2.1	1.6	2.3	2.4	2.5	1.6	1.8		
Gd	7.9	8.8	8.4	10.0	9.7	11.6	6.5	7.3		
Tb	1.1	1.5	1.1	1.6	1.7	1.8	1.1	1.2		
Dy	6.1	8.4	6.5	8.6	9.4	9.1	6.0	6.5		
Ho	1.1	1.5	1.2	1.5	1.6	1.6	1.2	1.3		
Er	3.2	3.9	3.3	4.1	4.3	4.4	3.4	3.7		
Tm	0.5	0.6	0.5	0.7	0.7	0.7	0.5	0.5		
Yb	3.3	4.1	3.3	4.1	4.3	4.2	3.7	3.7		
Lu	0.5	0.7	0.5	0.7	0.7	0.7	0.6	0.6		
Hf	5.9	9.4	4.8	7.4	7.3	8.1	8.0	6.8		

(continued)

Table 7 (continued)

Elements	KN11	KN12	KN15	KN16	KN17	KN18	KN19	KN20		
Ta	1.3	1.6	1.3	1.4	1.6	1.4	1.8	1.8		
Pb	23.7	23.2	26.6	26.7	25.5	23.6	35.5	17.3		
Th	22.4	26.4	22.2	23.8	26.5	27.4	18.3	18.3		
U	3.1	3.6	3.1	3.3	3.4	3.7	3.5	3.4		
La/Th	2.5	2.3	2.8	2.4	2.3	2.4	2.4	3.0		
La/Sc	3.7	4.9	3.9	3.7	3.7	3.6	2.9	3.5		
Th/Co	1.1	1.7	1.3	1.0	1.1	1.3	0.7	0.8		
Th/Sc	1.5	2.1	1.4	1.6	1.6	1.5	1.2	1.2		
\sum REE	263.9	280.8	278.1	287.0	306.0	327.2	211.2	269.3		
(Gd _N /Yb _N)	1.9	1.7	2.1	2.0	1.8	2.2	1.4	1.6		
Eu/Eu*	0.6	0.7	0.6	0.7	0.7	0.6	0.7	0.7		
Elements	KN21	KN22	KN23	KN24	KN25	KN26	KN27	KN28	KN29	KN30
Sc	10.9	11.6	10.2	11.7	15.9	16.5	15.7	14.5	16.0	16.1
V	112.0	105.9	115.7	99.2	121.9	128.2	136.2	146.6	137.6	141.5
Cr	106.4	100.2	108.1	101.7	118.2	105.8	114.5	129.2	117.0	124.9
Co	17.4	23.2	20.0	18.4	22.5	16.5	26.9	18.9	21.3	11.4
Ni	34.7	63.4	37.0	33.4	46.7	45.7	57.1	47.2	48.6	39.0
Cu	31.7	52.3	32.0	24.5	38.3	62.2	59.7	62.8	47.7	47.3
Zn	52.3	54.7	41.8	42.0	59.9	165.0	128.9	97.9	63.4	77.2
Ga	23.6	22.6	24.8	21.2	25.1	36.7	36.7	30.8	37.8	31.4
Rb	84.9	82.7	81.1	82.5	103.7	102.5	97.3	87.0	91.2	93.2
Sr	174.6	223.2	183.1	181.9	260.4	115.8	110.3	91.3	126.2	109.9
Y	17.2	20.1	17.3	21.6	33.3	28.3	26.7	22.6	26.9	26.4
Zr	207.6	224.9	217.9	392.0	333.3	220.1	220.6	211.0	216.9	237.1
Nb	20.7	19.7	20.8	23.3	26.4	25.5	25.7	26.4	28.1	25.9
Cs	4.5	2.9	4.9	2.9	4.5	6.5	6.4	5.6	6.0	5.8
Ba	340.1	452.1	314.0	505.3	694.7	361.5	367.6	335.4	382.4	395.7
La	43.7	38.8	41.4	45.2	49.2	55.2	58.9	55.0	66.3	51.9
Ce	108.1	95.1	114.6	112.0	109.6	107.6	111.0	101.8	124.5	91.3
Pr	9.7	9.9	9.3	10.8	11.1	15.0	14.8	13.7	14.8	11.7
Nd	33.2	36.6	31.9	38.4	39.8	57.4	52.5	47.2	53.2	40.7
Sm	5.9	7.2	5.6	6.9	8.0	10.0	8.9	7.6	10.0	7.1
Eu	1.1	1.5	1.1	1.4	1.9	2.1	1.8	1.5	2.0	1.4
Gd	4.7	5.9	4.5	5.4	7.4	10.3	8.7	7.3	8.9	6.7
Tb	0.7	0.9	0.7	0.9	1.2	1.3	1.2	1.0	1.3	1.0
Dy	3.9	4.9	3.8	4.8	6.6	6.7	6.2	5.6	6.3	5.7

(continued)

Table 7 (continued)

Elements	KN21	KN22	KN23	KN24	KN25	KN26	KN27	KN28	KN29	KN30
Ho	0.8	1.0	0.7	1.0	1.3	1.2	1.1	1.0	1.1	1.1
Er	2.2	2.6	2.1	2.9	3.7	3.2	3.1	2.8	3.1	3.1
Tm	0.3	0.4	0.3	0.4	0.5	0.5	0.5	0.4	0.5	0.5
Yb	2.2	2.6	2.1	3.1	3.7	3.3	3.1	2.8	3.1	3.2
Lu	0.4	0.4	0.3	0.5	0.6	0.5	0.5	0.4	0.5	0.5
Hf	4.9	5.3	5.0	9.2	7.6	6.9	7.0	6.4	7.4	7.4
Ta	1.6	1.5	1.6	3.1	2.2	1.6	1.7	1.7	2.2	1.5
Pb	15.4	14.3	15.5	13.6	21.0	25.0	23.2	23.1	26.4	19.1
Th	16.6	14.1	16.8	15.9	18.3	23.6	24.8	23.7	27.0	22.7
U	2.8	2.8	2.9	3.4	3.4	3.3	3.8	3.5	4.2	3.5
La/Th	2.6	2.8	2.5	2.8	2.7	2.3	2.4	2.3	2.5	2.3
La/Sc	4.0	3.3	4.1	3.9	3.1	3.4	3.7	3.8	4.1	3.2
Th/Co	1.0	0.6	0.8	0.9	0.8	1.4	0.9	1.3	1.3	2.0
Th/Sc	1.5	1.2	1.6	1.4	1.1	1.4	1.6	1.6	1.7	1.4
\sum REE	216.8	207.8	218.4	233.8	244.7	274.2	272.2	248.2	295.8	226.0
(Gd _N /Yb _N)	1.7	1.8	1.7	1.4	1.6	2.5	2.2	2.1	2.3	1.7
Eu/Eu*	0.7	0.7	0.7	0.7	0.7	0.6	0.6	0.6	0.7	0.6
Elements	KN31	KN32	KN33	KN34	KN35	KN36	KN37	KN38	KN39	KN40
Sc	13.9	17.6	4.4	15.6	15.9	15.9	15.4	20.6	12.8	7.6
V	116.2	146.6	164.1	155.1	117.7	116.2	123.4	171.4	115.9	125.5
Cr	109.1	100.1	131.1	127.0	105.5	100.8	109.6	129.4	91.0	100.7
Co	19.2	9.2	14.9	14.1	23.6	15.5	20.3	37.9	11.7	16.0
Ni	43.6	30.9	54.0	43.3	49.0	39.6	42.5	75.3	38.7	48.1
Cu	58.6	149.6	81.7	68.4	46.1	56.5	45.5	67.7	51.8	40.2
Zn	113.9	71.7	352.1	116.3	81.9	120.7	63.2	138.8	104.3	145.4
Ga	26.9	27.4	3.5	36.6	34.7	35.8	36.1	28.5	29.5	20.5
Rb	91.5	78.8	90.2	92.8	95.2	97.1	89.0	87.0	88.0	69.9
Sr	97.4	107.0	86.8	110.2	133.3	111.9	135.8	125.4	105.0	195.6
Y	21.1	32.3	23.4	25.5	23.3	29.3	29.8	47.6	28.9	12.7
Zr	238.0	231.8	176.6	193.4	236.6	279.7	239.5	237.9	223.3	218.8
Nb	23.0	22.6	21.9	24.7	25.9	27.4	27.1	23.1	23.7	20.1
Cs	4.9	5.0	5.5	6.2	6.1	6.6	5.2	5.1	5.8	2.9
Ba	420.4	450.2	304.1	339.5	399.1	396.0	398.8	388.3	427.4	220.2
La	55.8	60.1	45.4	56.2	52.2	60.6	64.0	57.8	60.8	24.5
Ce	100.6	113.1	88.8	107.2	90.2	116.1	118.5	118.3	113.7	58.5
Pr	13.1	15.6	12.5	14.4	11.2	15.5	14.1	16.7	15.4	6.2

(continued)

Table 7 (continued)

Elements	KN31	KN32	KN33	KN34	KN35	KN36	KN37	KN38	KN39	KN40
Nd	45.6	55.6	44.9	51.8	38.9	55.4	50.6	64.4	54.5	22.1
Sm	7.6	9.6	7.9	8.8	7.1	9.1	9.6	12.6	9.3	4.4
Eu	1.4	2.0	1.7	1.9	1.4	1.8	1.9	2.8	1.9	1.0
Gd	7.1	8.8	9.5	9.5	6.8	8.0	8.6	12.8	8.6	3.6
Tb	1.0	1.4	1.2	1.2	1.0	1.2	1.3	2.0	1.3	0.6
Dy	5.0	8.3	6.4	6.2	5.0	6.6	6.2	10.3	7.3	3.0
Ho	0.9	1.6	1.1	1.1	1.0	1.1	1.2	1.9	1.3	0.6
Er	2.5	4.3	3.2	3.0	2.7	3.1	3.2	5.0	3.7	1.7
Tm	0.4	0.7	0.5	0.5	0.5	0.5	0.5	0.7	0.6	0.3
Yb	2.5	4.5	3.2	3.0	2.9	3.1	3.2	4.5	3.7	1.8
Lu	0.4	0.7	0.5	0.5	0.5	0.5	0.5	0.7	0.6	0.3
Hf	7.2	8.3	0.6	6.0	7.8	8.9	8.0	6.7	7.6	5.1
Ta	1.5	1.5	0.3	1.4	1.9	1.8	2.1	1.4	1.6	1.5
Pb	20.0	20.0	19.2	23.7	25.4	24.4	22.8	21.0	23.0	21.5
Th	25.2	21.5	21.3	23.9	23.8	27.2	24.2	20.9	22.4	13.1
U	3.8	3.6	3.5	3.7	3.8	4.0	4.2	3.8	3.6	2.6
La/Th	2.2	2.8	2.1	2.4	2.2	2.2	2.6	2.8	2.7	1.9
La/Sc	4.0	3.4	10.2	3.6	3.3	3.8	4.1	2.8	4.7	3.2
Th/Co	1.3	2.3	1.4	1.7	1.0	1.8	1.2	0.6	1.9	0.8
Th/Sc	1.8	1.2	4.8	1.5	1.5	1.7	1.6	1.0	1.7	1.7
\sum REE	243.8	286.4	226.8	265.0	221.4	282.7	283.3	310.4	282.5	128.6
(Gd _N /Yb _N)	2.3	1.6	2.4	2.6	1.9	2.1	2.2	2.3	1.9	1.6
Eu/Eu*	0.6	0.7	0.6	0.6	0.6	0.6	0.6	0.7	0.7	0.7
Elements	KN41	KN42	KN43	KN44	KN45	KN46	KN47	KN48	KN49	KN50
Sc	7.4	11.0	12.3	8.0	6.6	10.4	8.7	13.5	10.6	9.2
V	119.5	125.4	109.7	95.2	100.9	118.3	111.3	137.6	122.5	155.0
Cr	106.4	113.6	96.9	85.8	86.4	101.3	90.2	106.0	97.2	121.7
Co	5.8	5.5	8.1	6.4	11.2	8.1	8.3	11.7	7.9	24.3
Ni	31.9	26.7	32.6	25.0	24.2	25.5	26.6	35.1	26.8	80.2
Cu	31.2	30.0	26.1	22.4	21.6	27.0	27.4	35.4	39.5	40.3
Zn	108.2	36.0	100.0	63.2	39.6	39.9	53.5	39.3	56.6	61.3
Ga	20.9	24.6	23.8	19.2	19.6	23.5	21.5	24.9	23.6	28.2
Rb	83.7	91.6	84.6	68.2	70.1	96.6	58.5	90.0	79.0	57.0
Sr	107.8	109.7	206.5	85.8	85.1	156.8	115.7	155.8	117.2	86.8
Y	11.2	13.9	21.9	9.4	9.2	15.6	9.7	21.3	14.1	8.5
Zr	221.7	226.0	199.5	226.1	174.2	199.9	188.8	204.4	187.2	207.5

(continued)

Table 7 (continued)

Elements	KN41	KN42	KN43	KN44	KN45	KN46	KN47	KN48	KN49	KN50	
Nb	22.3	25.7	22.2	21.0	20.6	23.1	22.8	22.9	23.0	23.7	
Cs	3.9	4.4	5.4	2.7	2.7	7.5	3.9	6.7	4.3	6.4	
Ba	181.7	233.9	289.3	177.6	165.3	185.6	159.0	228.4	201.8	120.2	
La	26.4	32.5	51.0	24.3	22.1	45.2	21.3	39.8	48.8	58.5	
Ce	56.8	74.4	102.6	53.5	49.9	93.5	64.8	93.1	103.2	119.1	
Pr	6.6	7.7	11.8	6.2	5.6	10.7	5.0	8.9	11.1	13.4	
Nd	23.2	26.7	42.2	22.0	19.8	38.3	17.3	30.7	39.4	48.8	
Sm	4.5	5.0	7.6	4.1	3.7	7.0	3.2	5.9	7.0	9.2	
Eu	0.9	1.0	1.6	0.8	0.7	1.4	0.6	1.2	1.5	2.1	
Gd	3.5	3.9	6.9	3.2	2.9	6.3	2.6	4.9	6.3	8.8	
Tb	0.6	0.6	0.9	0.5	0.5	0.8	0.4	0.8	0.8	1.2	
Dy	3.0	3.4	4.7	2.7	2.5	4.3	2.3	4.5	4.2	6.6	
Ho	0.6	0.7	0.9	0.5	0.5	0.8	0.5	0.9	0.8	1.3	
Er	1.6	1.9	2.5	1.5	1.4	2.5	1.3	2.5	2.3	4.7	
Tm	0.2	0.3	0.4	0.2	0.2	0.4	0.2	0.4	0.3	0.5	
Yb	1.6	2.1	2.4	1.6	1.5	2.4	1.5	2.7	2.3	3.3	
Lu	0.3	0.3	0.3	0.3	0.2	0.3	0.2	0.4	0.3	0.5	
Hf	5.2	5.4	4.8	5.3	4.2	4.9	4.6	4.8	4.5	4.9	
Ta	1.6	2.1	1.7	1.6	1.6	1.7	1.8	1.7	1.9	1.8	
Pb	15.8	16.0	14.0	14.4	13.2	12.9	13.9	16.2	15.4	17.1	
Th	14.4	16.0	17.1	14.6	12.5	15.9	13.4	17.1	16.5	7.0	
U	2.5	2.5	2.4	2.4	2.1	2.4	2.2	2.4	2.3	2.8	
La/Th	1.8	2.0	3.0	1.7	1.8	2.8	1.6	2.3	3.0	8.4	
La/Sc	3.6	3.0	4.1	3.0	3.4	4.4	2.5	2.9	4.6	6.3	
Th/Co	2.5	2.9	2.1	2.3	1.1	2.0	1.6	1.5	2.1	0.3	
Th/Sc	1.9	1.5	1.4	1.8	1.9	1.5	1.5	1.3	1.6	0.8	
\sum REE	129.6	160.6	235.7	121.4	111.5	213.9	121.3	196.8	228.4	277.9	
(Gd _N /Yb _N)	1.7	1.5	1.6	1.6	1.6	1.5	1.4	1.5	1.6	1.5	
Eu/Eu*	0.7	0.7	0.7	0.7	0.7	0.7	0.7	0.7	0.7	0.6	
Elements	KN51		KN52		KN53		KN54		KN55		Avg.
Sc	8.4		7.2		15.5		10.3		13.6		13.5
V	149.0		159.2		141.0		122.2		129.7		125.5
Cr	126.2		128.5		117.6		106.6		109.7		110.4
Co	14.9		12.4		11.3		11.6		16.9		17.3
Ni	42.5		43.9		33.5		30.5		31.5		43.6
Cu	42.8		27.3		29.8		26.8		30.3		53.1

(continued)

Table 7 (continued)

Elements	KN51	KN52	KN53	KN54	KN55	Avg.
Zn	60.2	46.7	40.0	49.7	33.1	112.0
Ga	28.5	29.8	27.3	24.8	26.0	27.3
Rb	72.3	19.7	104.0	91.8	104.6	92.4
Sr	128.2	71.7	137.6	213.0	208.0	162.2
Y	14.4	10.1	25.0	16.2	22.3	25.6
Zr	257.4	226.9	230.0	262.8	234.3	232.4
Nb	24.6	25.5	22.8	21.9	22.7	23.1
Cs	6.0	5.7	5.5	4.7	5.4	5.5
Ba	253.0	75.2	514.7	346.1	470.5	412.3
La	33.2	58.7	54.7	40.0	44.0	53.0
Ce	130.0	114.3	115.1	114.9	85.2	107.3
Pr	7.5	13.1	13.0	9.5	9.9	13.2
Nd	26.5	47.3	47.6	33.7	35.1	47.6
Sm	4.9	8.6	8.9	6.4	6.3	8.4
Eu	0.9	1.9	1.9	1.3	1.4	1.7
Gd	4.1	8.1	8.3	4.9	5.8	7.7
Tb	0.6	1.0	1.1	0.8	0.7	1.1
Dy	3.2	5.8	5.7	3.9	4.2	6.1
Ho	0.6	1.1	1.1	0.8	0.8	1.1
Er	1.7	3.2	3.1	2.1	2.5	3.2
Tm	0.2	0.5	0.4	0.3	0.4	0.5
Yb	1.7	3.1	2.9	2.2	2.6	3.2
Lu	0.3	0.4	0.4	0.4	0.4	0.5
Hf	6.1	5.3	5.4	6.1	5.6	6.5
Ta	1.8	2.1	1.8	1.7	1.7	1.6
Pb	16.3	12.1	16.4	14.7	13.9	20.6
Th	16.4	12.1	21.3	17.4	19.0	21.1
U	3.2	3.0	3.2	3.2	3.1	3.3
La/Th	2.0	4.9	2.6	2.3	2.3	2.6
La/Sc	3.9	8.1	3.5	3.9	3.2	4.1
Th/Co	1.1	1.0	1.9	1.5	1.1	1.4
Th/Sc	2.0	1.7	1.4	1.7	1.4	1.6
\sum REE	215.6	267.1	264.2	221.0	199.3	254.6
(Gd _N /Yb _N)	1.9	1.3	1.7	1.8	1.3	1.9
Eu/Eu*	0.6	0.6	0.7	0.7	0.7	0.7

Table 8 Trace element concentration in shale samples from Bhuj Formation

Elements	KB1	KB2	KB3	KB4	KB5	KB6	KB7	KB8	KB9
Sc	12.0	12.8	18.0	14.3	14.5	17.2	16.8	16.0	10.8
V	127.1	128.5	126.6	98.0	101.0	111.4	108.4	108.8	57.2
Cr	144.9	111.4	116.0	118.0	102.7	115.1	114.1	130.9	84.5
Co	16.1	13.7	26.6	16.4	22.9	21.3	20.5	16.5	16.1
Ni	32.2	30.6	44.6	49.6	41.1	42.2	38.3	42.9	35.9
Cu	29.5	28.7	34.8	30.4	33.9	39.0	35.1	84.9	20.4
Zn	47.1	54.1	64.1	53.1	100.0	79.0	50.7	120.8	31.6
Ga	29.5	29.3	28.1	22.6	19.0	23.6	22.5	24.2	14.0
Rb	95.3	94.2	99.0	89.6	74.4	92.5	87.4	89.3	85.8
Sr	100.2	101.8	129.3	130.4	59.1	67.9	67.3	76.2	76.4
Y	24.7	20.0	33.4	32.7	31.0	36.6	34.6	33.7	28.4
Zr	265.2	233.0	252.9	431.4	219.9	261.5	271.3	324.5	466.6
Nb	24.3	25.0	23.1	23.6	19.3	23.0	22.6	22.8	19.2
Cs	6.8	7.1	6.6	3.9	3.8	4.8	4.4	4.1	2.0
Ba	255.4	182.2	283.9	486.3	388.2	459.5	462.7	518.4	686.9
La	57.9	47.2	63.2	69.1	45.6	60.0	55.9	63.8	44.6
Ce	143.5	137.8	146.8	154.4	84.3	109.9	102.1	112.7	78.9
Pr	12.6	10.2	13.9	15.3	10.2	13.1	12.3	13.7	9.5
Nd	44.1	35.7	49.2	53.2	36.7	47.6	44.4	49.2	33.8
Sm	8.2	6.5	9.4	9.8	7.2	9.3	8.6	9.3	6.3
Eu	1.6	1.3	1.9	1.5	1.5	1.8	1.7	1.7	1.1
Gd	6.6	5.1	8.1	7.6	6.3	7.9	7.4	7.8	5.2
Tb	1.0	0.8	1.3	1.2	1.1	1.3	1.2	1.3	0.9
Dy	5.3	4.3	7.1	6.5	5.8	6.8	6.5	6.3	4.8
Ho	1.1	0.9	1.4	1.3	1.2	1.4	1.4	1.3	1.1
Er	2.9	2.4	3.9	4.0	3.4	4.0	3.9	3.7	3.1
Tm	0.4	0.3	0.5	0.6	0.5	0.5	0.5	0.5	0.4
Yb	2.8	2.4	3.9	4.5	3.3	3.8	3.8	3.5	3.1
Lu	0.5	0.4	0.6	0.8	0.5	0.6	0.6	0.6	0.5
Hf	6.2	5.7	6.2	10.1	6.2	7.6	7.8	9.4	13.2
Ta	1.9	2.2	1.9	1.8	1.2	1.7	1.7	1.8	1.3
Pb	12.4	14.1	17.1	14.9	35.4	22.3	17.9	27.4	14.6
Th	22.4	18.9	24.3	27.0	15.5	19.9	19.9	21.6	18.8
U	4.5	4.5	5.1	5.3	3.5	4.2	4.2	4.6	3.4
La/Th	2.6	2.5	2.6	2.6	2.9	3.0	2.8	3.0	2.4
La/Sc	4.8	3.7	3.5	4.8	3.2	3.5	3.3	4.0	4.1

(continued)

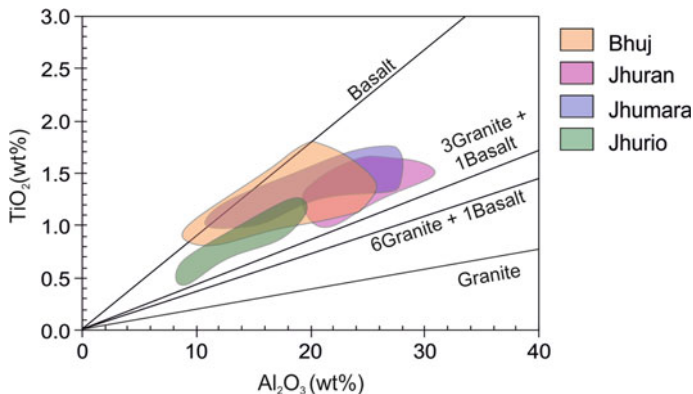
Table 8 (continued)

Elements	KB1	KB2	KB3	KB4	KB5	KB6	KB7	KB8	KB9
Th/Co	1.4	1.4	0.9	1.6	0.7	0.9	1.0	1.3	1.2
Th/Sc	1.9	1.5	1.4	1.9	1.1	1.2	1.2	1.3	1.7
\sum REE	288.5	255.3	311.3	329.8	207.6	268.0	250.3	275.3	193.4
(Gd _N /Yb _N)	1.9	1.7	1.7	1.4	1.5	1.7	1.6	1.8	1.4
Eu/Eu*	0.7	0.7	0.7	0.5	0.7	0.6	0.6	0.6	0.6
Elements	KB10	KB11	KB12	KB14	KB15	KB16	KB17	KB18	Avg.
Sc	9.3	8.8	14.5	11.4	13.0	17.7	12.7	17.5	13.9
V	51.0	54.7	111.8	90.0	114.3	115.9	93.0	95.4	99.6
Cr	61.0	69.5	109.9	93.9	108.3	128.7	122.0	157.1	111.1
Co	10.6	9.1	3.4	60.3	9.6	13.8	14.6	4.1	17.4
Ni	24.6	23.9	19.2	52.6	31.8	42.1	41.5	31.5	36.7
Cu	17.0	16.7	18.2	23.1	30.7	38.5	23.4	25.2	31.1
Zn	39.8	43.1	31.9	52.1	40.3	44.5	77.2	30.8	56.5
Ga	13.6	11.3	21.3	20.8	24.5	28.3	18.0	26.7	22.2
Rb	89.3	70.8	82.5	102.3	58.0	84.1	121.7	109.1	89.7
Sr	93.9	235.4	77.9	118.1	49.6	44.3	91.7	183.2	100.2
Y	21.0	18.4	28.0	21.4	33.3	24.6	34.2	42.1	29.3
Zr	343.2	410.7	277.5	215.5	335.8	217.6	552.1	481.4	327.1
Nb	17.4	16.9	22.6	18.3	24.2	26.0	20.6	28.6	22.2
Cs	1.5	0.9	4.3	3.8	6.0	8.9	4.1	3.0	4.5
Ba	822.0	768.4	453.4	801.3	262.4	219.2	847.1	1063.3	527.1
La	41.5	59.2	52.9	40.0	62.9	61.3	52.7	83.5	56.6
Ce	74.4	107.0	99.0	91.5	107.9	114.7	96.8	148.1	112.3
Pr	9.0	12.9	11.3	9.2	12.7	11.9	11.5	17.8	12.2
Nd	32.2	45.3	40.3	33.8	44.6	41.1	41.8	62.3	43.2
Sm	5.9	7.8	7.7	6.6	7.9	7.4	7.8	11.5	8.1
Eu	1.0	0.9	1.4	1.5	1.2	1.3	1.4	2.1	1.5
Gd	4.8	5.7	6.3	5.9	6.7	5.9	7.1	9.5	6.7
Tb	0.7	0.8	1.0	0.9	1.1	1.0	1.2	1.6	1.1
Dy	3.8	3.5	5.5	4.7	5.9	5.0	6.1	7.8	5.6
Ho	0.8	0.7	1.2	0.9	1.2	1.0	1.3	1.6	1.2
Er	2.3	2.1	3.3	2.4	3.5	2.8	3.7	4.6	3.3
Tm	0.3	0.3	0.5	0.3	0.5	0.4	0.5	0.6	0.4
Yb	2.3	2.0	3.4	2.2	3.4	2.5	3.6	4.4	3.2
Lu	0.4	0.3	0.5	0.4	0.5	0.4	0.6	0.7	0.5
Hf	9.6	12.1	8.3	5.0	9.5	6.3	15.3	14.0	9.0

(continued)

Table 8 (continued)

Elements	KB10	KB11	KB12	KB14	KB15	KB16	KB17	KB18	Avg.
Ta	1.3	1.2	1.9	1.3	2.0	2.1	1.6	2.1	1.7
Pb	17.5	17.1	15.0	9.8	21.0	22.2	29.7	37.4	20.3
Th	19.2	28.0	23.2	13.7	20.4	24.2	22.2	30.2	21.7
U	2.9	3.7	4.9	4.5	4.3	4.5	5.1	6.5	4.4
La/Th	2.2	2.1	2.3	2.9	3.1	2.5	2.4	2.8	2.6
La/Sc	4.5	6.7	3.7	3.5	4.8	3.5	4.1	4.8	4.2
Th/Co	1.8	3.1	6.7	0.2	2.1	1.7	1.5	7.4	2.1
Th/Sc	2.1	3.2	1.6	1.2	1.6	1.4	1.7	1.7	1.6
\sum REE	179.3	248.6	234.3	200.4	259.9	256.6	236.0	356.3	255.9
(Gd _N /Yb _N)	1.7	2.3	1.5	2.1	1.6	1.9	1.6	1.7	1.7
Eu/Eu*	0.6	0.4	0.6	0.7	0.5	0.6	0.6	0.6	0.6

**Fig. 3** Source rock discrimination based on TiO₂ versus Al₂O₃ plot (McLennan et al. 1979) for samples of Jhurio, Jhumara, Jhuran and Bhuj formations

of McLennan and Taylor (1991) (Fig. 15). However, a few samples of Jhuran and Bhuj formations occupy the Archean field.

On the basis of detrital zircon and monazite geochronology, Chaudhuri et al. (2020b) for the first time, report source rocks of Archean to Ordovician age (3300–400 Ma) located in the north and north-east of the basin contributed to the Mesozoic sedimentation in the Kutch Basin. While the majority of the age peaks indicate the dominance of post-Archean source rocks for these sediments, younger Jhuran and Bhuj formations exhibit additional older detrital zircon age peaks in the interval of 3300–2800 Ma. Chaudhuri et al. (2020c) report increasing mean T_{DM} in younger formations. Chaudhuri et al. (2020a) report zircon addition in the younger formations. The higher content of Hf in samples of Jhuran and Bhuj formations relates to the relatively high abundance of older zircon (Fig. 13). This increase in abundance of

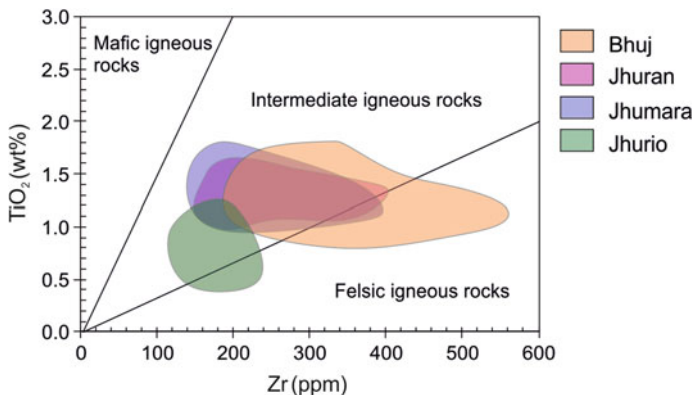


Fig. 4 Source rock discrimination based on TiO_2 versus Zr (ppm) plot (Hayashi et al. 1997) for samples of Jhurio, Jhumara, Jhuran and Bhuj formations

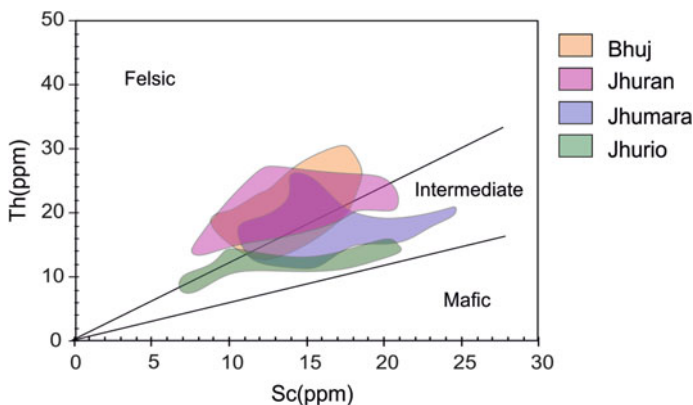


Fig. 5 Source rock discrimination based on Th versus Sc plot (Cullers 2002) for samples of Jhurio, Jhumara, Jhuran and Bhuj formations

older zircon in progressively younger formations indicates the erosional unroofing of older continental basement rocks at passive margins (Floyd and Leveridge 1987). The relationship between Cr and Ni distinguishes Early Archean, Late Archean and Post Archean source rocks (Taylor and McLennan 1985; Wronkiewicz and Condé 1987; McLennan et al. 1993; Etemad-Saeed et al. 2011; Wani and Mondal 2011). Mesozoic samples of Kutch support the predominance of the post-Archean source. Ratios of Eu/Eu^* and $(\text{Gd}_N/\text{Yb}_N)$ distinguish Archean and Post-Archean source rocks (McLennan and Taylor 1991; Armstrong-Altrin et al. 2004; Nagarajan et al. 2007; Singh 2010; Etemad-Saeed et al. 2011). The Mesozoic samples of Jhurio, Jhumara, Jhuran and Bhuj formations corroborate the dominance of post-Archean source rocks. The samples of Jhuran and Bhuj formations indicate sediments from Late Archean (Fig. 14) and Archean (Fig. 15) source rocks.

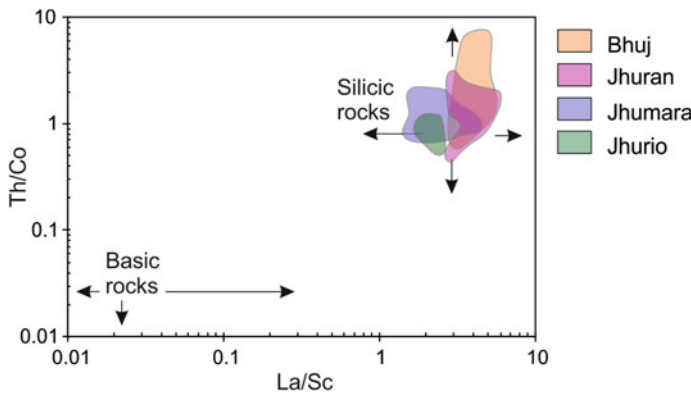
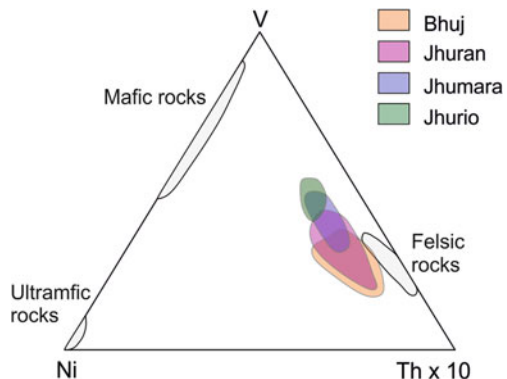


Fig. 6 Source rock discrimination based on Th/Co and La/Sc ratios (Cullers 2002) for samples of Jhurio, Jhumara, Jhuran and Bhuj formations

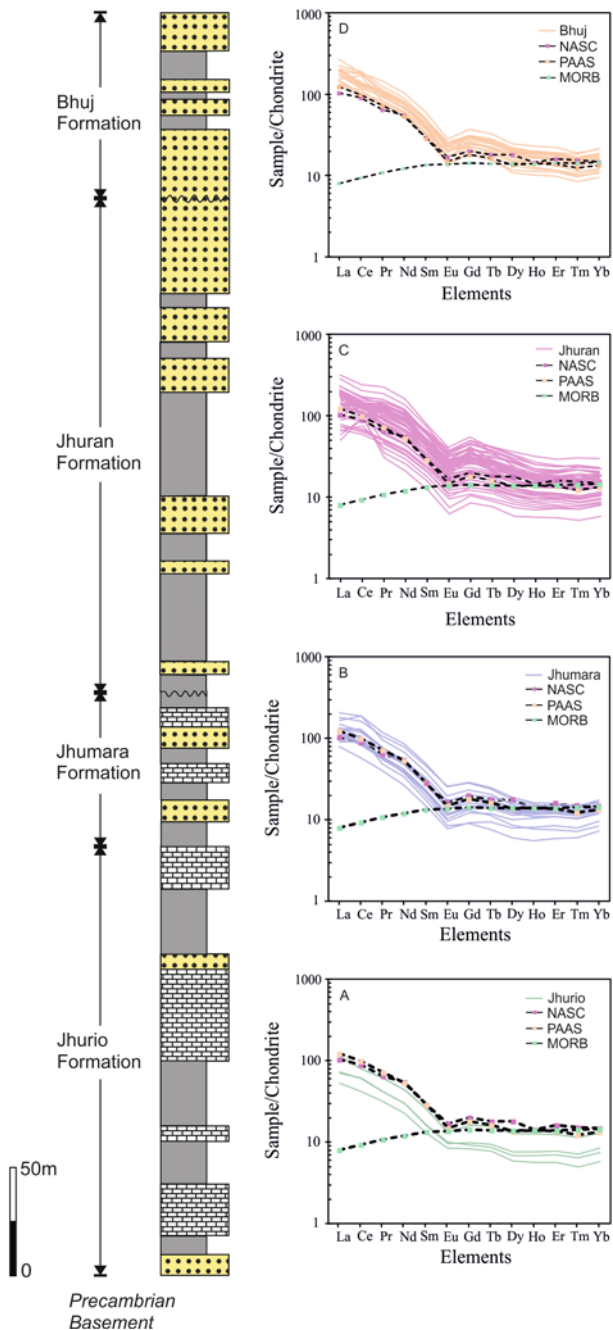
Fig. 7 Source rock discrimination based on V-Ni-Th $\times 10$ plot (Bracciali et al. 2007) for samples of Jhurio, Jhumara, Jhuran and Bhuj formations



Therefore, the geochemical data broadly supports the data from detrital geochronology. Petrographical evidence, heavy minerals, geochemical and geochronological proxies, and the overwhelmingly south-westerly paleocurrent patterns indicate that the potential source rocks existed northeast and north of the Kutch Basin. These include Precambrian rocks of the Aravalli craton and Nagar Parkar igneous complex (Chaudhuri et al. 2018, 2020a, b, c).

6 Conclusions

- (a) The diversity of the heavy minerals suggests multiple source rocks with evidence of a mixed clastic supply of first-cycle and recycled sandy particles. The ultra-stable rounded heavy detrital minerals could be an indicator



►Fig. 8 Composite litholog of the Jhurio, Jhumara, Jhuran and Bhuj formations in the Kutch Main-land (adapted from Biswas 2005; Fürsich et al. 2005; Mandal et al. 2016) along with the chondrite normalised REE patterns of samples of Jhurio, Jhumara, Jhuran and Bhuj formations (solid lines), NASC, PAAS and MORB (dashed lines). Chondrite meteorite values from Boynton (1983). NASC, PAAS and MORB values are from Haskin et al. (1968), Nance and Taylor (1976) and Sun and McDonough (1989), respectively

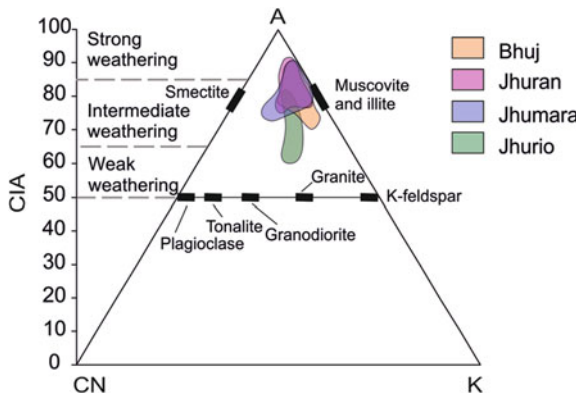


Fig. 9 A-CN-K plot (Nesbitt and Young 1982) indicating the extent of weathering for samples of Jhurio, Jhumara, Jhuran and Bhuj formations

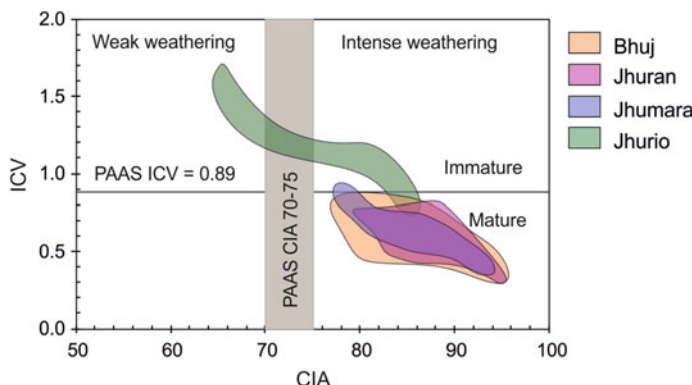


Fig. 10 CIA versus ICV indicating maturity and intensity of weathering (adapted from Long et al. 2012) for samples of Jhurio, Jhumara, Jhuran and Bhuj formations

of prolonged or intense transport other than indicators of the recycled detrital input.

- (b) Major oxides ($\text{SiO}_2/\text{Al}_2\text{O}_3$, $\text{Al}_2\text{O}_3/\text{TiO}_2$, $\text{K}_2\text{O}/\text{Na}_2\text{O}$) and trace elements (Zr, Th, Sc, Th/Co, Th/Sc and La/Sc) suggest the dominance of felsic source rocks. The LREE enriched chondrite-normalised REE pattern and the negative Eu

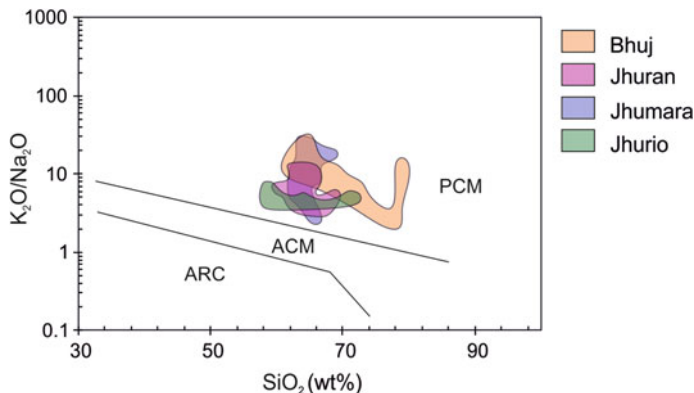


Fig. 11 Tectonic setting discrimination based on K_2O/Na_2O versus SiO_2 plot (Roser and Korsch 1986) for samples of Jhurio, Jhumara, Jhuran and Bhuj formations (PCM = Passive Continental Margin, ACM = Active Continental Margin, ARC = oceanic island arc margin)

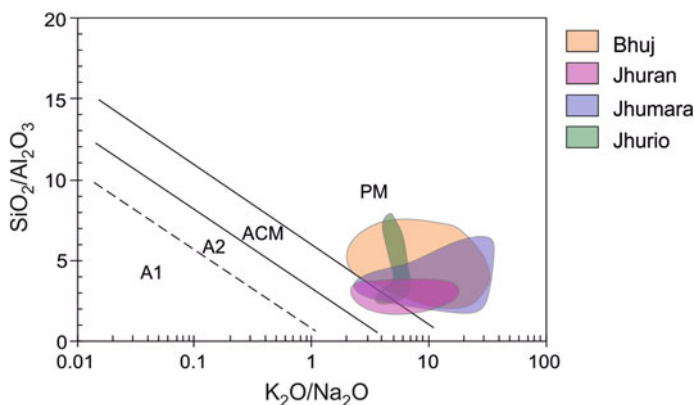


Fig. 12 Tectonic setting discrimination based on SiO_2/Al_2O_3 versus $\log(K_2O/Na_2O)$ plot (adapted from Maynard et al. 1982) for samples of Jhurio, Jhumara, Jhuran and Bhuj formations (PM = Passive continental Margin, ACM = Active Continental Margin, A1, A2 = oceanic island arc margin)

anomaly corroborate the predominance of felsic source rocks. However, the concentration of TiO_2 , Al_2O_3 , Zr , Th , Sc , suggest a minor mafic input in all samples. The concentrations of V and Ni highlight the presence of mafic input in the older Jhurio and Jhumara formations.

- (c) Chemical index of alteration (CIA), plagioclase index of alteration (PIA) and chemical index of weathering (CIW) indicate intermediate to strong weathering of sediments in Jhumara, Jhuran and Bhuj formations and a weak to intermediate weathering for sediments in the Jhurio Formation. The Index of compositional variability (ICV) suggests mature, recycled or highly weathered

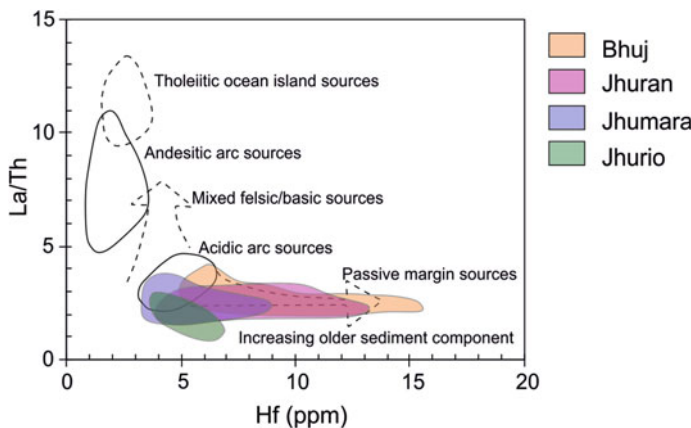


Fig. 13 Tectonic setting discrimination based on La/Th versus Hf plot (Floyd and Leveridge 1987) for samples of Jhurio, Jhumara, Jhuran and Bhuj formations

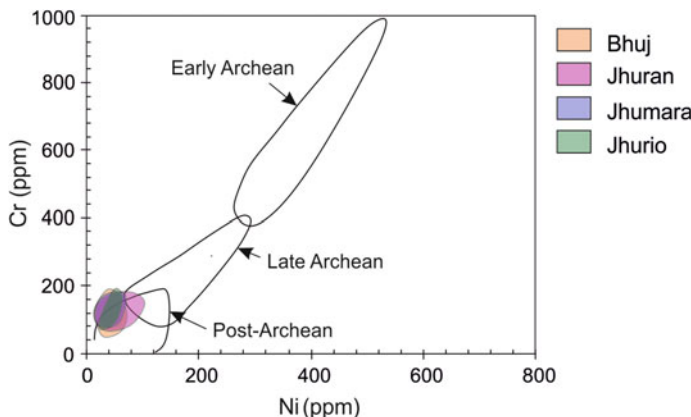


Fig. 14 Plot of Cr versus Ni (Taylor and McLennan 1985) for samples of Jhurio, Jhumara, Jhuran and Bhuj formations

first-cycle sediments in Jhumara, Jhuran and Bhuj formations and immature sediments in the Jhurio Formation.

- (d) Major oxides, their ratios (SiO_2 , $\text{SiO}_2/\text{Al}_2\text{O}_3$ and $\text{K}_2\text{O}/\text{Na}_2\text{O}$) and trace elements (La, Th and Hf) indicate a passive continental margin setting for the Mesozoic siliciclastic succession in Kutch Basin.
- (e) The concentration of Hf in samples of Jhuran and Bhuj formations highlights the presence of older input in younger formations suggesting erosional unroofing at the source.
- (f) Concentrations of Cr and Ni and the relationship between Eu/Eu^* and $(\text{Gd}_N/\text{Yb}_N)$ indicate the dominance of post-Archean rocks at source area.

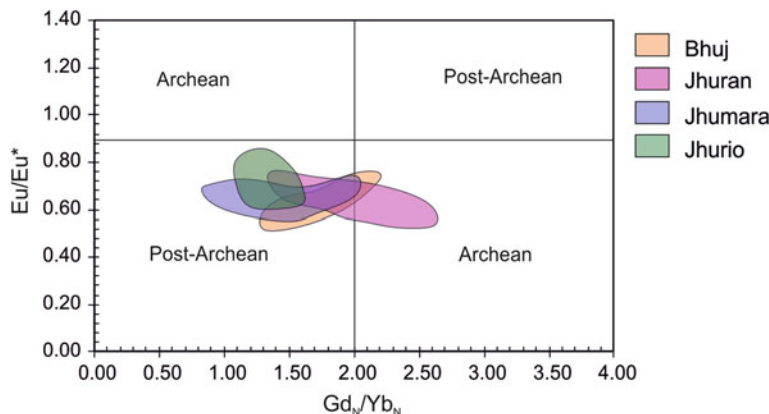


Fig. 15 Plot of Eu/Eu* versus (Gd_N/Yb_N) plot (McLennan and Taylor 1991) for samples of Jhurio, Jhumara, Jhuran and Bhuj formations

However, they also reveal older Archean or late Archean sediment input in younger Jhuran and Bhuj formations. The data corroborate the erosional unroofing, as suggested by Hf concentration. This also supports the results from detrital zircon and monazite geochronology and Nd isotopes in these sediments.

- (g) Heavy mineral and geochemical characteristics of Mesozoic sediments indicate Precambrian rocks of the Aravalli craton and Nagar Parkar igneous complex as sources of Mesozoic sediments in the Kutch Basin.

Acknowledgements AC and SB are thankful to IIT Bombay for the infrastructure support. ELP and GC acknowledge Università della Calabria and KSKV Kachchh University for the infrastructure support. SB acknowledges financial support from Science and Engineering Research Board, Government of India, through grant no. SR/S4/ES-709/2014.

References

- Ahmad AHM, Bhat GM (2006) Petrofacies, provenance and diagenesis of the Dhosa Sandstone Member (Chari Formation) at Ler, Kachchh sub-basin, Western India. *J Asian Earth Sci* 27:857–872
- Ahmad AHM, Noufal KN, Masroor AM, Khan T (2014) Petrography and geochemistry of Jumara Dome sediments, Kachchh Basin: implications for provenance, tectonic setting and weathering intensity. *Chinese J Geochem* 33:9–23
- Alberti M, Fürsich FT, Pandey DK (2013) Deciphering condensed sequences: a case study from the Oxfordian (Upper Jurassic) Dhosa Oolite member of the Kachchh Basin, western India. *Sedimentol* 60:574–598

- Amendola U, Perri F, Critelli S, Monaco P, Cirilli S, Trecci T, Rettori R (2016) Composition and provenance of the Macigno Formation (Late Oligocene-Early Miocene) in the Trasimeno Lake area (Northern Apennines). *Mar Pet Geol* 69:146–167
- Andò S, Garzanti E, Padoan M, Limonta M (2012) Corrosion of heavy minerals during weathering and diagenesis: a catalogue for optical analysis. *Sediment Geol* 280:165–178
- Armstrong-Altrin JS, Lee YI, Kasper Zubillaga JJ, Trejo Ramírez E (2017) Mineralogy and geochemistry of sands along the Manzanillo and El Carrizal beach areas, southern Mexico: implications for palaeoweathering, provenance and tectonic setting. *Geol J* 52:559–582
- Armstrong-Altrin JS, Lee YI, Verma SP, Ramasamy S (2004) Geochemistry of sandstones from the upper Miocene Kudankulam Formation, southern India: implications for provenance, weathering, and tectonic setting. *J Sed Res* 74:285–297
- Arora A, Banerjee S, Dutta S (2015) Black shale in late Jurassic Jhuran Formation of Kutch: possible indicator of oceanic anoxic event? *J Geol Soc India* 85:265–278
- Arora A, Dutta S, Gogoi B, Banerjee S (2017) The effects of igneous dike intrusion on organic geochemistry of black shale and its implications: Late Jurassic Jhuran Formation, India. *Int J Coal Geol* 178:84–99
- Bansal U, Banerjee S, Pande K, Arora A, Meena SS (2017) The distinctive compositional evolution of glauconite in the Cretaceous Ukra Hill Member (Kutch basin, India) and its implications. *Mar Pet Geol* 82:97–117
- Bhatia MR, Crook KA (1986) Trace element characteristics of graywackes and tectonic setting discrimination of sedimentary basins. *Contrib Min Pet* 92:181–193
- Biswas SK (1982) Rift basins in the western margin of India and their hydrocarbon prospects with special reference to Kutch basin. *AAPG Bull* 66:1497–1513
- Biswas SK (1987) Regional tectonic framework, structure and evolution of the western marginal basins of India. *Tectonophys* 135:307–327
- Biswas SK (1993) Geology of Kutch, vol 1. KDM Institute of Petroleum Exploration, Dehradun
- Biswas SK (2005) A review of structure and tectonics of Kutch basin, western India, with special reference to earthquakes. *Curr Sci* 88:1592–1600
- Biswas SK (1991) Stratigraphy and sedimentary evolution of the Mesozoic basin of Kutch, western India. In: Tandon SK, Pant CC, Casshyap SM (eds) *Stratigraphy and sedimentary evolution of western India*. Gyanodaya Prakashan, Nainital, pp 74–103
- Biswas SK (1977) Mesozoic rock stratigraphy of Kachchh. *Q J Geol Min Met Soc India* 49:1–52
- Biswas SK (1981) Basin framework, palaeo-environment and depositional history of the Mesozoic sediments of Kutch basin, western India. *Q J Geol Min Met Soc India* 53:56–85
- Boynton WV (1983) Cosmochemistry of rare earth elements: meteorite studies. In: Hendersen P (ed) *Rare earth element geochemistry*. Elsevier, pp 63–114
- Bracciali L, Marroni M, Pandolfi L, Rocchi S, Arribas J, Critelli S, Johnsson MJ (2007) Geochemistry and petrography of Western Tethys Cretaceous sedimentary covers (Corsica and Northern Apennines): from source areas to configuration of margins. *GSA Spec Pap* 420:73–93
- Chaudhuri A, Banerjee S, Chauhan G (2020a) Compositional evolution of siliciclastic sediments recording the tectonic stability of a pericratonic rift: Mesozoic Kutch Basin, western India. *Mar Petrol Geol* 111:476–495
- Chaudhuri A, Banerjee S, Le Pera E (2018) Petrography of Middle Jurassic to Early Cretaceous sandstones in the Kutch Basin, western India: implications on provenance and basin evolution. *J Palaeogeography* 7:2–14
- Chaudhuri A, Banerjee S, Prabhakar N, Das A (2020d) The use of heavy mineral chemistry in reconstructing provenance: a case study from Mesozoic sandstones of Kutch Basin (India). *Geol J*. <https://doi.org/10.1002/gj.3922>
- Chaudhuri A, Chatterjee A, Banerjee S, Ray JS (2020c) Tracing multiple sources of sediments using trace element and Nd isotope geochemistry: provenance of the Mesozoic succession in the Kutch Basin, western India. *Geol Mag*. <https://doi.org/10.1017/S0016756820000539>

- Chaudhuri A, Das K, Banerjee S, Fitzsimons ICW (2020b) Detrital zircon and monazite track the source of Mesozoic sediments in Kutch to rocks of Late Neoproterozoic and Early Palaeozoic orogenies in northern India. *Gond Res* 80:188–201
- Cox R, Lowe DR, Cullers RL (1995) The influence of sediment recycling and basement composition on evolution of mudrock chemistry in the southwestern United States. *Geochim Cosmochim Acta* 59:2919–2940
- Critelli S, Arribas J, Le Pera E, Tortosa A, Marsaglia KM, Latter KK (2003) The recycled orogenic sand provenance from an uplifted thrust belt, Betic Cordillera, southern Spain. *J Sed Res* 73:72–81
- Critelli S, Ingersoll RV (1994) Sandstone petrology and provenance of the Siwalik Group (northwestern Pakistan and western-southeastern Nepal). *J Sed Res* 64:815–823
- Crook KA (1974) Lithogenesis and geotectonics: the significance of compositional variation in flysch arenites (graywackes). In: Dott RH, Shaver RH (eds) Modern and ancient geosynclinal sedimentation. SEPM Spec Publ 19:304–310
- Cullers RL (2002) Implications of elemental concentrations for provenance, redox conditions, and metamorphic studies of shales and limestones near Pueblo, CO, USA. *Chem Geol* 191:305–327
- Cullers RL, Podkovyrov VN (2000) Geochemistry of the Mesoproterozoic Lakhanda shales in southeastern Yakutia, Russia: implications for mineralogical and provenance control, and recycling. *Precam Res* 104:77–93
- Desai BG, Biswas SK (2018) Postrift deltaic sedimentation in western Kachchh Basin: insights from ichnology and sedimentology. *Palaeo Palaeo Palaeo* 504:104–124
- Dickinson WR (1985) Interpreting provenance relations from detrital modes of sandstones. Provenance of arenites. Springer, Dordrecht, pp 333–361
- Dickinson WR, Suczek CA (1979) Plate tectonics and sandstone compositions. *AAPG Bull* 63:2164–2182
- Ding H, Ma D, Yao C, Lin Q, Jing L (2016) Implication of the chemical index of alteration as a paleoclimatic perturbation indicator: an example from the lower Neoproterozoic strata of Aksu, Xinjiang, NW China. *Geosci J* 20:13–26
- Etemad-Saeed NA, Hosseini-Barzi MA, Armstrong-Altrin JS (2011) Petrography and geochemistry of clastic sedimentary rocks as evidences for provenance of the Lower Cambrian Lalun Formation, Posht-e-badam block, Central Iran. *J African Earth Sci* 61:142–159
- Fedo CM, Wayne Nesbitt H, Young GM (1995) Unraveling the effects of potassium metasomatism in sedimentary rocks and paleosols, with implications for paleo-weathering conditions and provenance. *Geology* 23:921–924
- Floyd PA, Leveridge BE (1987) Tectonic environment of the Devonian Gramscatho basin, south Cornwall: framework mode and geochemical evidence from turbiditic sandstones. *J Geol Soc* 144:531–542
- Fürsich FT, Singh IB, Joachimski M, Krumm S, Schlierf M, Schlierf S (2005) Palaeoclimate reconstructions of the Middle Jurassic of Kachchh (western India): an integrated approach based on palaeoecological, oxygen isotopic, and clay mineralogical data. *Palaeo Palaeo Palaeo* 217:289–309
- Gu XX, Liu JM, Zheng MH, Tang JX, Qi L (2002) Provenance and tectonic setting of the Proterozoic turbidites in Hunan, South China: geochemical evidence. *J Sed Res* 72:393–407
- Harnois L (1988) The CIW index: a new chemical index of weathering. *Sediment Geol* 55:319–322
- Haskin LA, Haskin MA, Frey FA, Wildeman TR (1968) Relative and absolute terrestrial abundances of the rare earths. In: Ahrens LH (ed) Origin and distribution of the elements. Pergamon, pp 889–912
- Hayashi KI, Fujisawa H, Holland HD, Ohmoto H (1997) Geochemistry of ~1.9 Ga sedimentary rocks from northeastern Labrador, Canada. *Geochim Cosmochim Acta* 61:4115–4137
- Hubert JF (1962) A zircon-tourmaline-rutile maturity index and the interdependence of the composition of heavy minerals assemblages with the gross composition and texture of sandstones. *J Sed Pet* 32:440–450

- Kasanzu C, Maboko MA, Manya S (2008) Geochemistry of fine-grained clastic sedimentary rocks of the Neoproterozoic Ikorongo Group, NE Tanzania: implications for provenance and source rock weathering. *Precam Res* 164:201–213
- Long X, Yuan C, Sun M, Xiao W, Wang Y, Cai K, Jiang Y (2012) Geochemistry and Nd isotopic composition of the Early Paleozoic flysch sequence in the Chinese Altai, Central Asia: Evidence for a northward-derived mafic source and insight into model ages in an accretionary orogen. *Gond Res* 22:554–566
- López JMG, Bauluz B, Fernández-Nieto C, Oliete AY (2005) Factors controlling the trace-element distribution in fine-grained rocks: the Albian kaolinite-rich deposits of the Oliete Basin (NE Spain). *Chem Geol* 214:1–19
- Löwen K, Meinhold G, Güngör T (2018) Provenance and tectonic setting of Carboniferous-Triassic sandstones from the Karaburun Peninsula, western Turkey: a multi-method approach with implications for the Palaeotethys evolution. *Sediment Geol* 375:232–255
- Mandal A, Koner A, Sarkar S, Tawfik HA, Chakraborty N, Bhakta S, Bose PK (2016) Physico-chemical tuning of palaeogeographic shifts: Bhuj Formation, Kutch, India. *Mar Pet Geol* 78:474–492
- Mange MA, Maurer H (2012) Heavy minerals in colour. Chapman and Hall, London
- Maynard JB, Valloni R, Yu HS (1982) Composition of modern deep-sea sands from arc-related basins. *Geol Soc London Spec Pub* 10:551–561
- McDonald DA, Surdam RC (1984) Clastic diagenesis. *AAPG Memoir* 37:1–434
- McLennan SM (1993) Weathering and global denudation. *J Geol* 101:295–303
- McLennan SM, Fryer BJ, Young GM (1979) The geochemistry of the carbonate-rich Espanola Formation (Huronian) with emphasis on the rare earth elements. *Can J Earth Sci* 16:230–239
- McLennan SM, Taylor SR (1991) Sedimentary rocks and crustal evolution: tectonic setting and secular trends. *J Geol* 99:1–21
- McLennan SM, Hemming S, McDaniel DK, Hanson GN (1993) Geochemical approaches to sedimentation, provenance, and tectonics. *GSA Spec Pap*, pp 21–21
- McBride EF (1985) Diagenetic processes that affect provenance determinations in sandstone. In: Zuffa GG (ed) Provenance of arenites. NATO ASI Series (Series C: Mathematical and physical sciences). Springer, Dordrecht
- Mondal MEA, Wani H, Mondal B (2012) Geochemical signature of provenance, tectonics and chemical weathering in the Quaternary flood plain sediments of the Hindon River, Gangetic plain, India. *Tectonophys* 566:87–94
- Morton AC (1984) Stability of detrital heavy minerals in Tertiary sandstones of the North Sea Basin. *Clay Miner* 19:287–308
- Nagarajan R, Armstrong-Altrin JS, Nagendra R, Madhavaraju J, Moutte J (2007) Petrography and geochemistry of terrigenous sedimentary rocks in the Neoproterozoic Rabanpalli Formation, Bhima Basin, Southern India: implications for paleoweathering conditions, provenance and source rock composition. *J Geol Soc India* 70:297–312
- Nance WB, Taylor SR (1976) Rare earth element patterns and crustal evolution-I. Australian post Archean sedimentary rocks. *Geochim Cosmochim Acta* 40:1539–1551
- Nesbitt HW, Young GM (1982) Early Proterozoic climates and plate. *Nature* 299:715–717
- Ochoa M, Arribas ME, Arribas J, Mas R (2007) Significance of geochemical signatures of provenance in intracratonic rift basins: examples from the Iberian plate. In: Arribas J, Critelli S, Johnsson M (eds) Sedimentary provenance and petrogenesis: perspectives from petrography and geochemistry. *GSA Spec Pap* 420:99–219
- Paikaray S, Banerjee S, Mukherji S (2008) Geochemistry of shales from the Paleoproterozoic to Neoproterozoic Vindhyan Supergroup: implications on provenance, tectonics and paleoweathering. *J Asian Earth Sci* 32:34–48
- Le Pera E, Arribas J, Critelli S, Tortosa A (2001) The effects of source rocks and chemical weathering on the petrogenesis of siliciclastic sand from the Neto River (Calabria, Italy): implications for provenance studies. *Sedimentol* 48:357–378

- Periasamy V, Venkateshwari M (2017) Petrography and geochemistry of Jurassic sandstones from the Jhuran Formation of Jara dome, Kachchh basin, India: implications for provenance and tectonic setting. *J Earth Sys Sci* 126:1–20
- Quinby-Hunt MS, Wilde P (1991) The provenance of low-calcic black shales. *Mineral Deposit* 26:113–121
- Roser BP, Korsch RJ (1986) Determination of tectonic setting of sandstone-mudstone suites using content and ratio. *J Geol* 94:635–650
- Saha S, Banerjee S, Burley SD, Ghosh A, Saraswati PK (2010) The influence of flood basaltic source terrains on the efficiency of tectonic setting discrimination diagrams: an example from the Gulf of Khambhat, western India. *Sed Geol* 228:1–13
- Saha S, Burley SD, Banerjee S (2018) Mixing processes in modern estuarine sediments from the Gulf of Khambhat, western India. *Mar Pet Geol* 91:599–621
- Schieber J (1992) A combined petrographical-geochemical provenance study of the Newland Formation, Mid-Proterozoic of Montana. *Geol Mag* 129:223–237
- Scholle PA, Schlüger PR (1979) Aspects of diagenesis. *SEPM Spec Pub* 26
- Singh P (2010) Geochemistry and provenance of stream sediments of the Ganga River and its major tributaries in the Himalayan region, India. *Chem Geol* 269:220–236
- Sun W, McDonough WF (1989) Chemical and isotopic systematics of oceanic basalts: implications of mantle composition and processes. *Geol Soc London Spec Pub* 42:313–345
- Taylor SR, McLennan SM (1985) The continental crust: its composition and evolution. Blackwell Scientific Publications, Oxford
- Wang C, Zhang L, Dai Y, Lan C (2015) Geochronological and geochemical constraints on the origin of clastic meta-sedimentary rocks associated with the Yuanjiacun BIF from the Lüliang Complex, North China. *Lithos* 212:231–246
- Wani H, Mondal MEA (2011) Evaluation of provenance, tectonic setting, and paleoredox conditions of the Mesoproterozoic-Neoproterozoic basins of the Bastar craton, Central Indian Shield: using petrography of sandstones and geochemistry of shales. *Lithosphere* 3:143–154
- Worden RH, Burley SD (2003) Sandstone diagenesis: the evolution of sand to stone. In: Burley SD, Worden RH (eds) *Sandstone diagenesis: recent and ancient*. International Association of Sedimentologists, Blackwell Publishing, pp 1–44
- Wronkiewicz DJ, Condie KC (1987) Geochemistry of Archean shales from the Witwatersrand Supergroup, South Africa: source-area weathering and provenance. *Geochim Cosmochim Acta* 51:2401–2416
- Yan Z, Wang Z, Yan Q, Wang T, Guo X (2012) Geochemical constraints on the provenance and depositional setting of the Devonian Liuling Group, East Qinling Mountains, Central China: implications for the tectonic evolution of the Qinling Orogenic Belt. *J Sed Res* 82:9–20
- Zhu W, Zheng B, Shu L, Ma D, Wu H, Li Y, Huang W, Yu J (2011) Neoproterozoic tectonic evolution of the Precambrian Aksu blueschist terrane, northwestern Tarim, China: insights from LA-ICP-MS zircon U-Pb ages and geochemical data. *Precam Res* 185:215–230
- Zuffa GG (1987) Unravelling hinterland and offshore paleogeography from deep-water arenites. In: Leggett JK, Zuffa GG (eds) *Deep-marine clastic sedimentology: concepts and case studies*. Graham and Trotman, London, pp 39–61